

# Syndrome aware mitigation of logical errors

Dorit Aharonov,<sup>1,2</sup> Yosi Atia,<sup>1</sup> Eyal Bairey,<sup>1</sup> Zvika Brakerski,<sup>1,3</sup> Itsik Cohen,<sup>1</sup> Omri Golan,<sup>1,\*</sup> Ilya Gurwich,<sup>1</sup> Netanel H. Lindner,<sup>1,4</sup> and Maor Shutman<sup>1</sup>

<sup>1</sup>Qedma Quantum Computing, Tel Aviv, Israel

<sup>2</sup>The Benin School of Computer Science and Engineering, Hebrew University, Jerusalem, Israel

<sup>3</sup>Faculty of Mathematics and Computer Science, Weizmann Institute of Science, Israel

<sup>4</sup>Department of Physics, Technion, Haifa, Israel

Broad applications of quantum computers will require *error correction* (EC). However, quantum hardware roadmaps indicate that physical qubit numbers will remain limited in the foreseeable future, leading to residual logical errors that limit the size and accuracy of achievable computations. Recent work suggested *logical error mitigation* (LEM), which applies known *error mitigation* (EM) methods to logical errors, eliminating their effect at the cost of a runtime overhead. Improving the efficiency of LEM is crucial for increasing the logical circuit volumes it enables to execute.

We introduce *syndrome-aware logical error mitigation* (SALEM), which makes use of the syndrome data measured during error correction, when mitigating the logical errors. The runtime overhead of SALEM is exponentially lower than that of previously proposed LEM schemes, resulting in significantly increased circuit volumes that can be executed accurately. Notably, relative to the routinely used combination of error correction and syndrome rejection (post-selection), SALEM increases the size of reliably executable computations by orders of magnitude. In this practical setting in which space and time are both resources that need to be optimized, our work reveals a surprising phenomenon: SALEM, which tightly combines EC with EM, can outperform physical EM even above the standard fault-tolerance threshold. Thus, SALEM can make use of EC in regimes of physical error rates at which EC is commonly deemed useless.

## I. INTRODUCTION

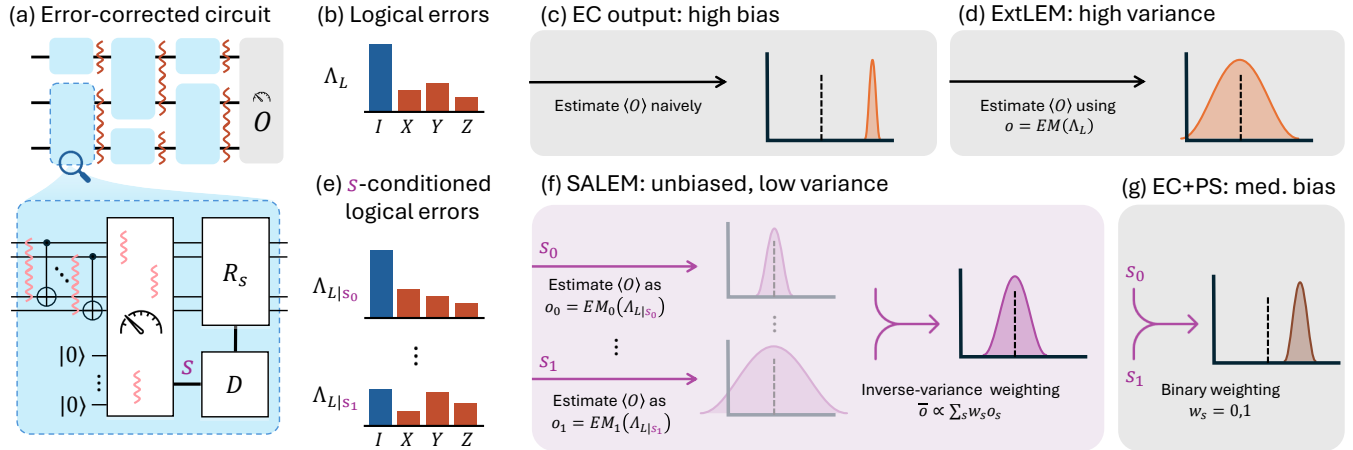
Quantum computation promises dramatic algorithmic speedups ('quantum advantages', QAs) over classical computation, for a variety of applications [1]. Fulfilling this promise requires a solution to the problem of errors in quantum processing units (QPUs) which quickly accumulate to render even small quantum computations useless. The detrimental effect of errors is commonly agreed to be the main bottleneck towards realizing QAs.

The long-term solution for errors in QPUs is fault tolerant (FT) quantum computation [2–5], where logical qubits used in quantum algorithms are redundantly encoded onto physical qubits by a quantum error correcting code [6–9] such that dominant errors can be detected and inverted during computation. Recent experiments have made significant progress towards realizing error correction (EC), but are still focused on few-qubit logical circuits, and have so far demonstrated limited improvements in error rates due to EC [10–19]. This is due to the value of the physical error rates of current QPUs ( $\epsilon \sim 10^{-3}$ , that is, a physical error every  $\sim 10^3$  physical operations), as well as the limited number of physical qubits currently available, ranging from tens to hundreds. Recent theoretical advances have made significant strides towards more efficient EC schemes [20–23], predicting logical error rates as low as  $\epsilon_L \sim 10^{-5} - 10^{-8}$  (per logical qubit) with physical error rates of near-term hardware [24–29]. But even these logical error rates will

not suffice to maintain the high output accuracies needed for many applications in and beyond the 'MegaQuOp' regime (circuits with  $\sim 10^6$  logical gates) [30], where the first QAs of significant industry relevance may be anticipated [31]. More generally, for as long as high-fidelity physical qubit numbers remain limited, the logical error rates achievable with EC will restrict accessible logical circuit volumes (number of logical gates) and output accuracies, and thus the applicability of quantum computing [30].

An alternative near-term solution for hardware errors is termed 'quantum error mitigation' (EM) [32–38] and is now standard practice when working with QPUs. In EM, the execution of a given ideal (error-free) quantum circuit is replaced with multiple executions of (generally distinct) noisy circuits, the outcomes of which are post-processed to yield an estimate for the outcome of the ideal circuit. In terms of resources, EM therefore requires little or no overhead in physical qubit number, but instead implies an overhead in the number of circuit executions ('shots'), which translates to an overhead in QPU time. It is expected that QPUs paired with EM protocols will soon provide the first *useful* finite QAs [30, 39–42], and there are already claims that EM has reliably estimated the output of ideal quantum circuits that cannot be simulated with super-computers in reasonable time [43–46]. The required shot overhead for EM is generically exponential in the total infidelity, i.e., the product of the error rate per gate  $\epsilon$  and the circuit volume  $V$  [30, 47–51]. This overhead still allows EM to accurately execute circuits with volumes  $V \sim (1-10)\epsilon^{-1}$ , yielding a significant boost over execution without EM which is limited to circuits of volumes  $V \sim \delta\epsilon^{-1}$ , where  $\delta$  is the required ac-

\* [omri.golan@qedma.com](mailto:omri.golan@qedma.com)



curacy. With near-term error rates  $\epsilon \sim 10^{-3}$ , this limits EM to circuit volumes  $V \sim 10^3 - 10^4$ , which is expected to suffice for surpassing classical simulation, but not for applications of major industry relevance.

EM can similarly be used to boost the circuit volumes of error-corrected quantum circuits. The combination of the two approaches was recently proposed [52–56] and very recently demonstrated [57]. We refer to this general approach as ‘logical error mitigation’ (LEM). In terms of resources, LEM uses available QPU time *and* physical qubit numbers, to maximize accessible circuit volume and output accuracy. The LEM methods described in the literature thus far may be summarized as follows: First, apply EC to replace physical gates by corresponding FT logical gates with a reduced error rate. Then apply EM to these logical gates, as if they are physical gates. We refer to this approach as ‘external LEM’ (ExtLEM), as it does not ‘look inside’ the logical gates, and specifically, does not make use of the syndrome data measured within them. The volumes enabled by ExtLEM can be estimated by  $V \sim (1 - 10)\epsilon_L^{-1}$  where  $\epsilon_L$  is the logical error rate. These volumes are significantly larger than  $V \sim \delta\epsilon_L^{-1}$  enabled by EC alone. Improving the runtime incurred by ExtLEM, and thus the enabled volumes, is

critical in order to accelerate the path towards QAs of major industry relevance.

In this work we follow up on an idea alluded to in our previous work [30], and introduce *syndrome-aware logical error mitigation* (SALEM), which exploits the syndrome data measured within logical gates as part of EC (the approach works also for error detection, but we focus here on EC). SLEM makes use of syndrome data in order to achieve a reduced shot overhead compared to ExtLEM, and consequently enables larger circuit volumes and output accuracies, given fixed resources. A ‘fine-grained’ version of SLEM is depicted in Fig. 1, and compared to EC (alone), ExtLEM and the standard combination of EC and post-selection (EC+PS) [58, 59]. Figure 2 demonstrates the performance improvements of SLEM, achieved already with a simple ‘coarse-grained’ version of SLEM, where syndromes are grouped to a small number of subsets (some of which may be rejected).

Figure 2(a) demonstrates the behavior of estimators due to different error reduction methods as a function of circuit volume. In this example, SLEM maintains the required accuracy  $1 - \delta = 99\%$  at volumes over  $2 \times$  larger than with ExtLEM,  $20 \times$  larger than with EC+PS, and  $200 \times$  larger than with EC. Figure 2(b) shows how this

boost in circuit volume (CVB) [30], measured relative to bare circuit execution (Bare), changes with the required accuracy, showing that the advantage of SALEM over ExtLEM is essentially independent of  $\delta$ , while the advantage over EC and EC+PS, which are bias-limited, grows with the required accuracy, as  $\sim \delta^{-1}$ .

The performance of LEM relative to physical EM depends on the physical error rate  $\epsilon$ , which determines the logical error rate  $\epsilon_L$ . In Fig. 2(a)-(b),  $\epsilon$  is significantly below the ‘FT (pseudo) threshold’, defined by the break-even condition  $\epsilon_L(\epsilon) = \epsilon$ ; such that  $\epsilon_L \ll \epsilon$ , and EC is much better than bare circuit execution (Bare). Accordingly, ExtLEM, and more so SALEM, significantly outperform physical EM (with  $3\times$  and  $6\times$  larger accessible volumes in this example).

Importantly, in the context of LEM, the FT threshold no longer marks the point at which EC becomes beneficial. Instead, we regard new (pseudo) thresholds as more relevant: these are the physical error rate values at which ExtLEM and SALEM, respectively, become preferable to using physical EM. Figure 2(c) shows estimation errors for different methods at physical error rates around the FT threshold, revealing the new thresholds. Due to the space-time overhead of EC, both the ExtLEM and SALEM thresholds are volume-dependent (see Appendix 11). The ExtLEM threshold is always lower than the FT threshold, and approaches it at large volumes. However, the SALEM threshold is always higher than the ExtLEM threshold. Importantly, for sufficiently large circuit volumes, it *surpasses the FT threshold*, and continues to *increase* with volume. As shown in Fig. 2, the SALEM threshold exceeds the FT threshold already at practical volumes of  $O(1/\epsilon_L)$ . Thus, through SALEM, the use of EC can be beneficial even in a regime where EC is not expected to be useful, namely, *above* the standard FT threshold.

## II. SETUP

Consider an error-corrected logical circuit  $C$ , as shown in Fig. 1(a). The circuit implements logical gates onto logical qubits, encoded in a larger number of physical qubits. Within each logical gate, a syndrome bit-string  $s$  (‘local syndrome’) is measured, and subsequently decoded to obtain a corresponding recovery operation. With high probability, the recovery is successful, and no logical error, corresponding to an unwanted logical gate, occurs. Logical operations are usually constructed to be ‘fault tolerant’ to some order  $t$  ( $t$ -FT), such that events including up to  $t$  physical errors (‘faults’) are properly recovered from, and logical errors are due to events including  $\geq t+1$  physical errors. The probability distribution  $\mathbb{P}(\sigma)$  of possible logical errors  $\sigma$  defines the *logical error channel*  $\Lambda_L = \sum_\sigma \mathbb{P}(\sigma)\sigma$ , see Fig. 1(b). Note that defining logical channels which are accurate enough for prediction and mitigation of error-corrected circuits is subtle. We refer to Appendix 1 for our definition and

its justification. Given the channel  $\Lambda_L$ , the corresponding *logical error rate*  $\epsilon_L = 1 - \mathbb{P}(\sigma = I)$ , which is the probability for a non-trivial logical error per logical gate, can be viewed as the limiting factor for the performance of EC. In particular, the expectation value  $\langle O \rangle_{\Lambda_L}$  of a logical operator  $O$  measured at the end of the circuit will generically deviate from its ideal (error-free) value  $\langle O \rangle = \langle O \rangle_I$ ; where the ‘global channel’  $\Lambda_L$  denotes the list of logical error channels associated with all logical gates in the circuit  $C$ . Naive estimation of  $\langle O \rangle$ , by averaging over the measured values of  $O$  in  $N$  shots, will produce the biased outcome  $\langle O \rangle_{\Lambda_L}$  in expectation, with a variance  $\leq 1/N$ , see Fig. 1(c).

LEM protocols are designed to eliminate the bias  $b = |\langle O \rangle_{\Lambda_L} - \langle O \rangle|$  due to logical errors, at the expense of a shot overhead. Proposed ExtLEM methods (Fig. 1(d)) do this by applying a fixed EM protocol  $EM$  to all shots, designed to mitigate the global channel  $\Lambda_L$ , and producing an estimator  $o$  that depends on this channel [52–57]. The protocol  $EM$  is *unbiased* (possibly, for a specific instance) if it reproduces the ideal result in expectation,  $\mathbb{E}[o] = \langle O \rangle$ . The cost of this estimation is a *shot overhead*  $\Gamma$  – defined through a given upper bound  $\mathbb{V}[o] \leq \Gamma/N$  on the variance  $\mathbb{V}[o]$  as a function of the number of shots  $N$  used to produce  $o$ .

## III. FINE-GRAINED SALEM

We start by discussing a ‘fine-grained’ version of SALEM (FG-SALEM), in which each syndrome is treated separately. FG-SALEM reuses the syndrome data generated within logical operations, by (i) separately mitigating shots in which distinct syndromes were measured, and (ii) properly averaging over the resulting per-syndrome estimates.

Restricting attention to shots in which a particular syndrome  $s$  is measured, the relevant error channel is the  $s$ -conditioned logical error channel,  $\Lambda_{L|s} = \sum_\sigma \mathbb{P}(\sigma|s)\sigma$  (Fig. 1(d)). In fact, logical error channels in error-corrected circuits can generally be conditioned on syndromes measured in past and even future logical gates. Importantly, we prove that logical error channels can be approximated to leading order by conditioning only on syndrome data measured in nearby logical gates (see Appendix 2). We keep the notation  $\Lambda_{L|s}$  for simplicity, though  $s$  in this notation should be understood as including past and future syndrome data relevant to the particular logical gate. We collect the local syndromes measured in all logical gates in the circuit to a ‘global syndrome’  $\mathbf{s}$ , and denote the list of all conditioned logical channels in the circuit as an ‘ $\mathbf{s}$ -conditioned global logical error channel’  $\Lambda_{L|\mathbf{s}}$ . We note that mapping  $s \mapsto \Lambda_{L|s}$  (or  $\mathbf{s} \mapsto \Lambda_{L|\mathbf{s}}$ ) is a challenging computational problem, discussed in Sec. IV.

Given  $N_s$  shots (out of a total of  $N$ ) in which a particular  $\mathbf{s}$  is observed, FG-SALEM applies an EM protocol  $EM_{\mathbf{s}}$  designed to mitigate  $\Lambda_{L|\mathbf{s}}$ , and produces an esti-

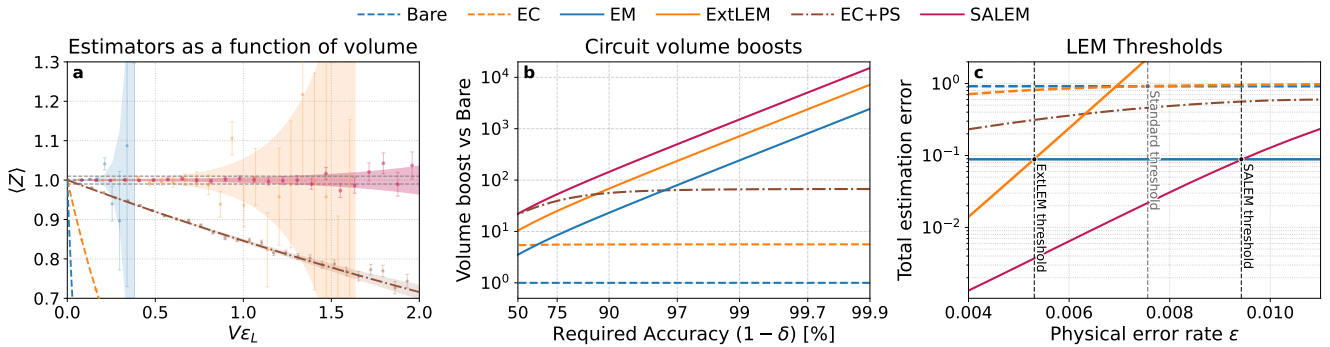


FIG. 2. Performance benefits of (coarse-grained) SALEM. (a) Comparison of estimators for an expectation value  $\langle Z \rangle$  due to different error reduction methods, as a function of logical circuit volume  $V$ , normalized with the logical error rate  $\epsilon_L \approx 10^{-4}$ , for a fixed physical error  $\epsilon = 10^{-3}$ . EC is based on a distance 4 surface code memory circuit subject to circuit-level physical errors, see Fig. 3 and Appendix 10 for technical details. All error reduction methods are allocated the same space and time overheads, relative to the number of qubits and the runtime needed to meet the allowed estimation error (1%, gray dashed lines) in an idealized error-free QPU. Specifically, we allocate a space-time volume corresponding to one-hundred error-corrected shots per error-free shot. The physical methods Bare and EM exploit the given space overhead by parallelizing shots, and have a lower shot time than methods involving EC. Shaded bands show the expected statistical spread of estimators (mean  $\pm$  one standard deviation), with mean curves shown only for biased methods and points illustrating a representative finite-shot realization. SALEM outperforms all methods, maintaining the required accuracy for significantly larger circuit volumes. (b) The ‘circuit volume boost’ (CVB) is the multiplicative improvement in achievable volume for a given required accuracy [30]. Methods limited by bias (EC and EC+PS), can provide significant CVBs, which do not change much with allowed inaccuracy  $\delta$ . Methods limited by statistical errors (EM, ExtLEM and SALEM), provide a CVB  $\sim \delta^{-1}$ , and are therefore superior at small  $\delta$  (high required accuracy). SALEM achieves the largest circuit volumes among all methods, at both high and low accuracy. (c) The behavior of estimation errors (including both biases and statistical errors) for the different methods as a function of physical error rate reveals the standard ‘FT (pseudo) threshold’ (gray dot), as well as two new types of (pseudo) thresholds, obtained by comparing ExtLEM and SALEM to physical EM (black dots). The logical circuit volume is scaled relative to the physical error rate,  $V = 2.5/\epsilon$ , such that the Bare and EM methods have constant estimation errors. At practical volumes  $V = O(1/\epsilon_L)$ , the SALEM threshold is larger than the FT threshold.

mator  $o_s$  (Fig. 1(f)). Note that a non-zero  $N_s$  may be as low as 1. In this section we thus restrict attention to ‘single-shot’ protocols  $EM_s$ , that can produce an estimator  $o_s$  using even a single shot. This restriction is not required for ‘coarse-grained’ SALEM (CG-SALEM), discussed below.

In particular, we consider protocols  $EM_s$  that (in expectation) invert  $\Lambda_{L|s}$  locally, by sampling from quasi-probability (QP) distributions [32, 34, 41, 60]; or that sample informationally-complete measurement bases and invert  $\Lambda_{L|s}$  globally, in (extensive) post-processing [61, 62]. Note that FG-SALEM with local inversion is adaptive, modifying the executed circuit in real time based on the already-measured part of  $s$ , generalizing the syndrome-dependent recovery operation of EC. Accordingly, in this case the logical error channel for a given logical gate is conditioned on syndrome data from logical gates in its past lightcone. In contrast, in FG-SALEM based on global inversion, logical channels are applied in post-processing and may therefore be conditioned also on syndromes in the future lightcone. Both types of protocols require characterization of the channels  $\Lambda_{L|s}$ , and are in principle unbiased if this characterization is exact. The primary examples we study in this paper are based on local inversion protocols, as their shot over-

head is well understood, they do not inherently require extensive classical computation, and they apply straightforwardly even to local channels  $\Lambda_{L|s}$  with a large (order-1) infidelity  $\epsilon_{L|s}$  - which generically appear in EC and are important for SALEM.

If all protocols  $EM_s$  are unbiased, each  $o_s$  reproduces  $\langle O \rangle$  in expectation,  $\mathbb{E}[o_s] = \langle O \rangle$ , but with a different shot overhead  $\Gamma_s$ , defined by  $\mathbb{V}[o_s] \leq \Gamma_s/N_s$  (Fig. 1(f)). An aggregated estimator  $\bar{o} \propto \sum_s w_s o_s$  is then constructed as a weighted average over syndrome subsets, with weights  $w_s$ . The estimator  $\bar{o}$  is unbiased for any choice of weights, which may therefore be chosen to minimize the FG-SALEM shot overhead  $\Gamma_{SALEM}^{FG}$ , defined by  $\mathbb{V}[\bar{o}] \leq \Gamma_{SALEM}^{FG}/N$ . As shown in Appendix 3, the optimal choice is given by ‘inverse-variance’ (IV) weights  $w_s = N_s/\Gamma_s$ , and the shot overhead for the resulting  $\bar{o}$  is given (up to negligible corrections) by the ‘harmonic expectation’ of  $\Gamma_s$  over  $s$ ,

$$\Gamma_{SALEM}^{FG} = \mathbb{H}[\Gamma_s] := \mathbb{E}[\Gamma_s^{-1}]^{-1}. \quad (1)$$

The FG-SALEM shot overhead in Eq. (1) is significantly lower than that of ExtLEM, assuming both are based on the same underlying EM protocol. To gain intuition for this statement, assume the underlying EM protocol satisfies the simplified but representative functional relation  $\Gamma(\epsilon) = e^{\lambda V \epsilon}$ , between the infidelity  $\epsilon$  of

the mitigated error channel (averaged over all  $V$  gates in the circuit), and the corresponding shot overhead  $\Gamma$ . The parameter  $\lambda$  appearing in the exponent (and thus, strongly affecting the shot overhead), is an order-1 coefficient that may be referred to as the ‘blowup rate’ of the EM protocol. Thus, the shot overhead for ExtLEM is  $\Gamma_{ExtLEM} = e^{\lambda V \epsilon_L}$ , and the shot overheads for FG-SALEM are  $\Gamma_s = e^{\lambda V \epsilon_{L|s}}$ . Noting that  $\epsilon_L = \mathbb{E}[\epsilon_{L|s}]$ , we have  $\Gamma_{ExtLEM} = e^{\lambda V \mathbb{E}[\epsilon_{L|s}]} = e^{\mathbb{E}[\log \Gamma_s]} = \mathbb{G}[\Gamma_s]$ , which is the ‘geometric expectation’ of  $\Gamma_s$ . The well known HM-GM inequality then shows that

$$\Gamma_{SALEM}^{FG} = \mathbb{H}[\Gamma_s] \leq \mathbb{G}[\Gamma_s] = \Gamma_{ExtLEM}, \quad (2)$$

with the gap determined by the non-uniformity of  $\Gamma_s$ , and hence of  $\epsilon_{L|s}$ . These are generically highly non-uniform in error-correcting circuits, since the appearance of different syndromes requires different minimal numbers of faults  $m_s \leq t + 1$ , such that  $\mathbb{P}(s) \sim \epsilon^{m_s}$ , and  $\epsilon_{L|s} \sim \epsilon^{t+1-m_s}$  are separated into different orders in  $\epsilon$ . In particular, the ‘worst’ syndromes, with  $m_s = t + 1$ , are responsible for a significant part of the gap between  $\Gamma_{SALEM}^{FG}$  and  $\Gamma_{ExtLEM}$ , see Appendix 8. Generalizing Eq. (2), Appendix 5 shows that  $\Gamma_{SALEM}^{FG} \leq \Gamma_{ExtLEM}$  corresponds to a generalized mean inequality, which holds under mild convexity assumptions satisfied by a wide variety of EM protocols.

Many EM protocols show an approximately-exponential behavior, with blowup rate  $\lambda = \lim_{\epsilon \rightarrow 0} (\epsilon V)^{-1} \log \Gamma(\epsilon)$ . Table I shows numerical estimates for the FG-SALEM blowup rate  $\lambda_{SALEM}^{FG} = \lim_{\epsilon_L \rightarrow 0} (\epsilon_L V)^{-1} \log \Gamma_{SALEM}^{FG}$  in a number of examples based on QP distributions, exhibiting a significant improvement over  $\lambda_{ExtLEM} = \lambda = 4$ . For each code in Tab. I we consider a fixed EC circuit, augmented with either a ‘realistic’ decoder, considered fast enough to run in real time, or the optimal *degenerate maximum likelihood* (ML) decoder, which gives the lowest possible logical error  $\epsilon_L$  for the chosen EC circuit [63]. We see that FG-SALEM has a lower blowup rate for realistic decoders. This seemingly positive result implies a subtle interplay between FG-SALEM and optimal decoding, which we now discuss.

#### IV. FINE-GRAINED SALEM AS AN EXTENSION OF OPTIMAL DECODING

The implementation of FG-SALEM requires solving the ‘syndrome-conditioned logical characterization’ problem: compute  $\Lambda_{L|s}$  given  $s$ . Doing this to high accuracy is feasible for codes with a small number of possible syndromes, like the distance-3 codes in Table I. However, for large codes, this is generally intractable, as it is at least as hard as ML decoding, which is a  $\#P$ -hard computational task [66]. Indeed, given the channel  $\Lambda_{L|s} = \sum_{\sigma} \mathbb{P}(\sigma|s) \sigma$  one can perform ML decoding by extracting the most likely logical error  $\sigma_s = \operatorname{argmax}_{\sigma} \mathbb{P}(\sigma|s)$ .

TABLE I. Blowup rates for FG-SALEM based on QP distributions, in distance-3 codes. For each code we consider a FT logical memory circuit, equipped with a realistic sub-optimal decoder (minimal-weight perfect matching, MWPM [64], or a minimal-weight lookup table, LUT [65]) or the optimal ML decoder, and subjected to a circuit-level noise model. Values for  $\lambda_{SALEM}^{FG}$  are to be contrasted with the blowup rate for ExtLEM,  $\lambda = 4$ . To make this comparison explicit, we also report the shot-overhead improvement factor  $\Gamma_{ExtLEM}/\Gamma_{SALEM}^{FG} = \exp((4 - \lambda_{SALEM}^{FG})\Lambda)$  at fixed normalized volume  $\Lambda := V\epsilon$  (here  $\Lambda = 3$ ).

Code	Surface		Steane		
	Decoder	MWPM	ML	LUT	ML
$\lambda_{SALEM}^{FG}$		2.3	3.3	2.5	3.0
$\Gamma_{ExtLEM}/\Gamma_{SALEM}^{FG}$		164	8.17	90.0	20.1

We can now explain why  $\lambda_{SALEM}^{FG}$  is lower for the realistic decoders in Tab. I: The local inversion of  $\Lambda_{L|s}$  can be viewed as first implementing  $\sigma_s^{-1}$  without a shot overhead, and subsequently inverting the channels  $\sigma_s^{-1} \Lambda_{L|s}$  obtained after ML decoding. Thus, the shot overhead  $\Gamma_{SALEM}^{FG}$  is independent of the decoder, implicitly improving it to ML. However, the logical error  $\epsilon_L$  is larger for realistic decoders, leading to a smaller blowup rate  $\lambda_{SALEM}^{FG}$  in the realistic case.

Conceptually, we see that idealized FG-SALEM (i.e., with exact characterization) is a generalization of ML decoding - inverting the entire error channel  $\Lambda_{L|s}$  as opposed to ‘just’ the most likely error  $\sigma_s$ . Just as ML decoding is used to define the optimal performance to which realistic decoders aspire to, and which can be approached in exchange for classical complexity, we view idealized FG-SALEM as marking an extreme point in the tradeoff between quantum complexity (shot overhead) and classical complexity.

FG-SALEM may be practical for certain large codes by leveraging TN decoders, which perform an approximate syndrome-conditioned logical characterization, see the discussion section. In the following section we take an alternative approach towards a scalable implementation of SALEM.

#### V. COARSE-GRAINED SALEM

We consider two modifications of the FG-SALEM protocol discussed so far. These modifications define ‘coarse-grained’ SALEM (CG-SALEM) protocols, that can reach blowup rates close to those of FG-SALEM, without requiring significant real-time classical computation, beyond what is already used by realistic decoders, see Fig. 3. Moreover, CG-SALEM relaxes the limitations on the types of EM protocols which can be used, and can even be made compatible with any EM protocol.

Our first modification is to allow coarse-graining of the set of global syndromes. This is achieved by partition-

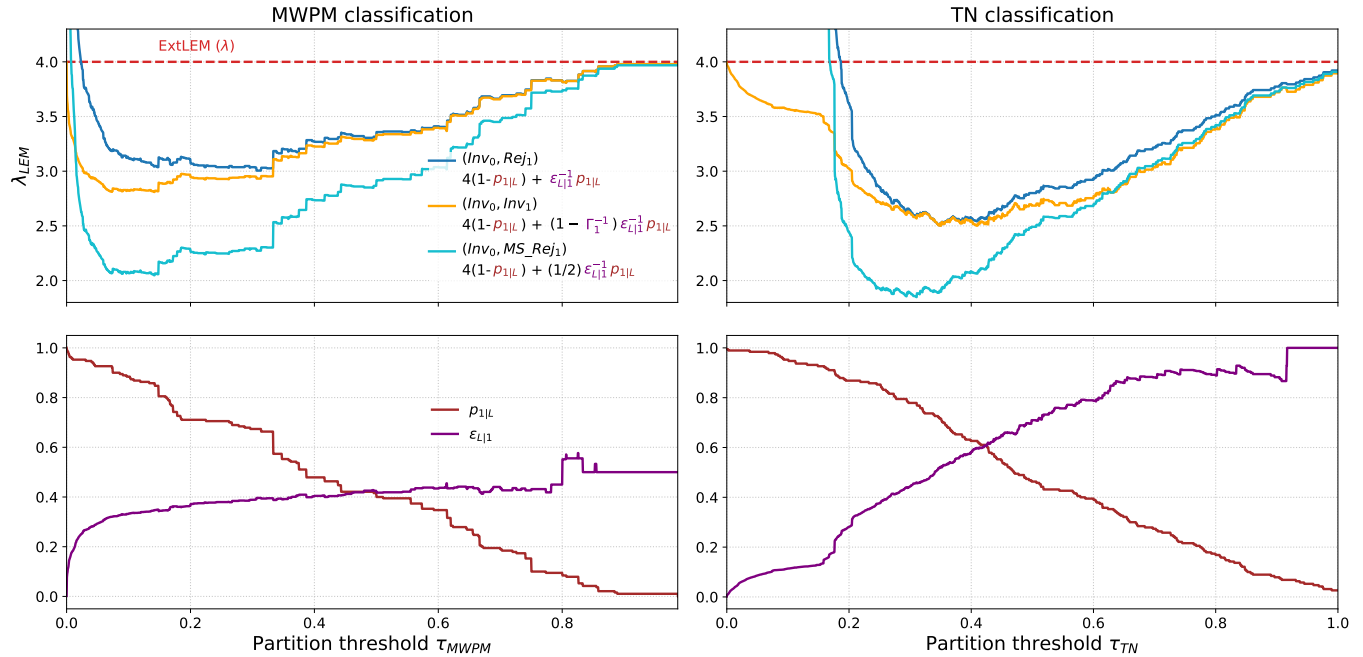


FIG. 3. Performance of coarse-grained (binary) SALEM. Top panels: Blowup rates  $\lambda_{SALEM}^{\{S_0, S_1\}}$  for different variants of CG-SALEM based on binary partitions  $S = S_0 \cup S_1$  of syndromes ('binary CG-SALEM'). The 'good' set  $S_0$  should have a small conditioned logical error  $\epsilon_{L|0}$ , and is mitigated using local inversion (Inv<sub>0</sub>). The 'bad' set  $S_1$  should have a large conditioned logical error  $\epsilon_{L|1}$ , and is mitigated by rejection (blue), local inversion (orange) or mid-shot rejection (cyan). In each panel, the bad set  $S_1$  shrinks from  $S$  to  $\emptyset$  along the x-axis. Minimal values of  $\lambda_{LEM}$  for each binary CG-SALEM variant indicate the optimal partition for that variant. The (Inv<sub>0</sub>, Inv<sub>1</sub>) variant always improves upon both ExtLEM (based on local inversion) and (Inv<sub>0</sub>, Rej<sub>1</sub>), but requires that classification be performed in real-time and does not significantly improve upon (Inv<sub>0</sub>, Rej<sub>1</sub>) when using (near-) optimal partitions. Mid-shot rejection also requires a real-time classifier, and (Inv<sub>0</sub>, MS\_Rej<sub>1</sub>) can provide the best blowup rate (of QPU time) among the three variants, depending on the depth of the mitigated logical circuit (data shown corresponds to depth  $D = \epsilon_L^{-1}$ ). The data is obtained from simulations of logical memory circuits for the  $d = 4$  surface code, decoded using the MWPM algorithm [64], representing a sub-optimal 'realistic' decoder. We consider two families of classifiers: one based on the MWPM decoder itself (Left Panels) [58, 67, 68], which can therefore run in real-time; and a stronger but slower family of classifiers based on a TN decoder (Right Panels) [69], which may only be possible to run in post-process. The x-axes correspond to a threshold that defines a specific classifier within each family, setting a cutoff on a decoder-derived proxy for the conditional logical error (see Appendix 10). Numerically obtained blowup rates are well approximated by simple expressions in terms of  $\epsilon_{L|1} = \mathbb{P}(\text{logical error}|S_1)$  and  $p_{1|L} = \mathbb{P}(S_1|\text{logical error})$ , the latter representing the fraction of logical errors 'contained' in the set  $S_1$  (see top legend and Appendix 8-9). These quantities are plotted in the Bottom Panels. Maximizing both  $\epsilon_{L|1}$  and  $p_{1|L}$  is desirable but impossible, and optimal partitions are obtained when the two are balanced.

ing each set of local syndromes  $S = \{s\}$  (namely, syndromes associated with a specific logical gate) to subsets  $S_k$ ,  $k = 0, 1, \dots, K$ , such that  $S = \bigcup_{k=0}^K S_k$ . Collecting all local subset indices  $k$  we obtain a global index  $\mathbf{k}$ , and global syndrome subsets  $S_{\mathbf{k}}$ . Given such a partition, CG-SALEM will apply an EM protocol  $EM_{\mathbf{k}}$  designed to mitigate the channel  $\Lambda_{L|\mathbf{k}}$ , to the  $N_{\mathbf{k}}$  shots in which syndromes  $s \in S_{\mathbf{k}}$  are measured, obtaining an estimator  $o_{\mathbf{k}}$ . The CG-SALEM estimator  $\bar{o}$  will then be obtained as a weighted average of  $o_{\mathbf{k}}$  with IV weights  $w_{\mathbf{k}} = N_{\mathbf{k}}/\Gamma_{\mathbf{k}}$ , where  $\Gamma_{\mathbf{k}}$  is a bound on the shot overhead of  $EM_{\mathbf{k}}$ . Note that more generally, one can directly partition the set of global syndromes.

The second modification is the possible rejection of  $S_K$ , implemented by assigning a weight  $w_{\mathbf{k}} = 0$  to global indices  $\mathbf{k}$  including at least one instance of  $K$ . This may be viewed as a limiting case of IV weighting, with infinite

shot overhead  $\Gamma_{\mathbf{k}} \rightarrow \infty$  assigned to such global indices  $\mathbf{k}$ .

In analogy with Eq. (1), coarse-graining with IV weighting leads to the shot overhead  $\Gamma_{SALEM}^{\{S_{\mathbf{k}}\}} = \mathbb{H}[\Gamma_{\mathbf{k}}]$ . In analogy with Eq. (2), this overhead is always better than ExtLEM, but worse than FG-SALEM,  $\Gamma_{SALEM}^{FG} \leq \Gamma_{SALEM}^{\{S_{\mathbf{k}}\}} \leq \Gamma_{ExtLEM}$ , with finer partitions providing an overhead which is closer to FG-SALEM. Rejecting  $S_K$  further increases the shot overhead to  $\Gamma_{SALEM}^{\{S_{\mathbf{k}}\}, Rej} = \mathbb{P}_{Acc}^{-1} \mathbb{H}[\Gamma_{\mathbf{k}} | Acc] \geq \Gamma_{SALEM}^{\{S_{\mathbf{k}}\}}$ , where  $\mathbb{P}_{Acc}$  is the (global) acceptance probability. An equality occurs if  $\Gamma_{\mathbf{k}} = \infty$  for all rejected  $\mathbf{k}$ . Note however, that since final measurements from rejected shots are not used, such shots can in principle be rejected once the first rejected local syndrome is measured. Such 'mid-shot rejection' does not change the shot overhead, but we find that it can significantly reduce QPU time overheads, for circuits with

practically relevant volumes and aspect ratios (Appendix 9). Thus, when minimizing QPU time as opposed to shot number, the optimal SALEM protocol would include a subset of syndromes that are mid-shot rejected, while accepted syndromes would be completely partitioned to singletons, as in FG-SALEM.

A main advantage of CG-SALEM over FG-SALEM is that mapping syndromes to corresponding logical error channels is computationally trackable for large codes. Indeed, instead of the syndrome-conditioned logical characterization ( $s \mapsto \Lambda_{L|s}$ ) needed for FG-SALEM, which may be computationally hard, CG-SALEM requires two computationally tractable tasks:

**Partition and classification:** Define a partition  $S = \cup_k S_k$ , and classify each measured syndrome  $s$  to its containing subset  $S_k$ . Useful partitions should preserve a significant fraction of the shot-overhead improvement of FG-SALEM over ExtLEM, and allow for computationally efficient classification,  $s \mapsto k$ . We find that such useful partitions can be constructed using ‘soft-output decoders’ [58, 67, 68, 70]. In addition to proposing a recovery operation, such decoders produce a metric  $\tau$  for the probability of a logical error given the proposed recovery. Fig. 3 shows the performance of CG-SALEM with partitions based on the value of  $\tau$ .

**Subset-conditioned characterization:** Estimate the channels  $\Lambda_{L|k}$  for (accepted subsets)  $k = 0, \dots, K$ . We focus on small numbers  $K$  of subsets, such that all channels  $\Lambda_{L|k}$  can be efficiently computed in pre-processing and stored in a short lookup table. We sketch our characterization procedure in Appendix 2, and provide a detailed account elsewhere [71].

CG-SALEM offers several additional advantages over FG-SALEM. First, if the protocols  $EM_s$  require adaptive logic, the reduction to a smaller number of protocols  $EM_k$  simplifies this logic. For example, mapping  $s$  to a sample from a corresponding QP distribution for  $\Lambda_{L|k}^{-1}$  can be done efficiently for a small number of subsets. Note that mid-shot rejection is adaptive, as opposed to standard rejection. Second, coarse graining and rejection may be used to ensure that all (accepted) subsets  $S_k$  are probable enough to implement protocols  $EM_k$  requiring a large number of shots in order to produce an estimator, such as ZNE.

We observe that for  $K = 0$  (no partition) we reproduce ExtLEM. The case  $K = 1$  (binary partition) with a rejected subset  $S_1$  and a complementary accepted subset  $S_0$ , to which a trivial protocol  $EM_0 = \text{do\_nothing}$  is applied, corresponds to the commonly used combination of EC and post-selection (EC+PS) [58, 59] (Fig. 1(g)). A significant drawback of EC+PS is that it leaves unmitigated the accepted error channels  $\Lambda_{L|0}$ , leading to a bias  $b = |\langle O \rangle - \langle O \rangle_{\Lambda_{L|0}}|$ . An additional drawback is that the shot overhead  $\mathbb{P}_{acc}^{-1}$  for mitigating the channels  $\Lambda_{L|1}$  by rejection is sub-optimal, unless  $\Gamma_k = \infty$  for all  $k \neq 0$ . Such divergences happen when the rejected channel  $\Lambda_{L|1}$  is singular, see Appendix 8.

The simplest novel instance of SALEM is obtained for

$K = 1$  by assigning a non-trivial protocol  $EM_0$  to the accepted set  $S_0$  (and rejecting  $S_1$ ). As demonstrated in Fig. 2, this already suffices to achieve a significant advantage over both ExtLEM and EC+PS. With a single accepted set, this version of SALEM is compatible with *any* protocol  $EM_0$ , which can be performed non-adaptively in all shots, while classification and rejection can be performed in post-processing. If classification is nevertheless performed in real-time, adaptivity can be used to reduce quantum runtime, by either (i) accepting and mitigating the set  $S_1$ , or (ii) rejecting it mid-shot, once a syndrome  $s \in S_1$  is observed. In Fig. 3 we compare these different variants of CG-SALEM based on binary partitions, demonstrating the tradeoffs between classical real-time processing and quantum runtime (see Appendices 8–10 for details).

## VI. DISCUSSION AND OUTLOOK

EM on the physical level plays a key role in working with existing QPUs, extending the circuit volumes that can be executed accurately by orders of magnitude. Likewise, LEM is expected to similarly play a key role in utilizing error-corrected QPUs for as long as physical qubit numbers remain limited [30, 42]. In this work we demonstrated that LEM can be made significantly more efficient, by re-purposing the syndrome data generated as part of EC. Effectively using this data requires syndrome classifiers, which are closely related to a growing body of work on ‘soft-output decoders’ [58, 67, 68, 70]. Thus, SALEM is intimately connected with EC, and we believe the two should be viewed holistically, as a framework that maximizes output accuracy given an allowance of physical qubits, quantum runtime, and classical compute resources for real-time processing, as well as for pre- and post-processing.

Rapid progress has been made recently in experimental demonstrations of EC [10, 12, 72]. We anticipate the focus of such experiments to gradually shift from demonstrating an improvement over noisy circuit execution, to demonstrating the more practically relevant improvement over physical EM using SALEM. The ‘SALEM threshold’ we defined corresponds precisely to this comparison. We find, perhaps counterintuitively, that despite the large space-time overhead of EC, the efficiency of SALEM can make EC useful even in noise rate regimes where EC (alone) does not improve upon bare circuit execution. Moreover, SALEM can provide practical value in the very near term, when applied to QPUs supporting tens of *error detected* logical qubits, which are already becoming available to end users [10, 73].

Our work identifies several directions for further research. First, in our numerical simulations, we focused on well studied EC codes, namely color and surface codes, where SALEM could be simulated on top of well known fault-tolerance constructions and decoders, with publicly accessible implementations. It would be interesting to

estimate the performance of SALEM on top of more recently proposed EC schemes [20–22]. Second, we found that in non-adaptive instances of SALEM, a ‘strong but slow’ TN decoder operating in post-processing can be useful for syndrome classification. We relied on the recent work of Ref. [69], that extended TN decoders to the circuit-level setting. In doing so we found that run times for TN decoders must be significantly improved if they are to be practically used, even in post-processing. Reference [74] demonstrated a significant speedup for TN decoders in the code-capacity setting, and it would be interesting to extend this approach to the circuit level. With fast and accurate enough TN decoders, it may even be possible to perform FG-SALEM, since these decoders can be used to approximate the required channels  $\Lambda_{L|s}$ . Finally, in Appendix 7 we show that SALEM can have a shot overhead that is lower than that of any possible LEM protocol that does not make use of syndrome data (i.e., any ExtLEM protocol). Whether or not SALEM makes optimal use of syndrome data, and accordingly, whether syndrome-based LEM methods that are more efficient than SALEM exist, is an interesting and practically relevant open question.

**Acknowledgments** We thank our colleagues at Qedma and John Preskill for insightful discussions and helpful feedback during this project.

**Competing interests** This work describes methods that are the subject of U.S. and international patent applications filed by Qedma Quantum Computing Ltd. [71].

**Note added** While finalizing this manuscript, References [75, 76] appeared on the arXiv, discussing LEM based on soft-output decoders. Ref. [75] describes the special case of binary CG-SALEM with a rejected subset, in the code-capacity setting, where no faults occur during error correction. Ref. [76] describes EC+PS, as well as a LEM protocol based on heuristic post-processing of syndrome-resolved data.

## APPENDIX

The following appendices provide a technical overview. Further details, including detailed definitions and proofs, can be found in Ref. [71].

1. Logical error channels	9
2. Temporally-local approximate logical error-channels	10
3. Fine-grained SALEM	12
4. FG-SALEM with QP distributions	12
5. Advantage of FG-SALEM over ExtLEM	13
6. CG-SALEM	14
7. Violation and derivation of lower bounds for shot overheads in LEM	14
8. Case study: Binary CG-SALEM with QP distributions	14
9. Mid-shot rejection	16
10. Numerical simulations	17
a. Steane code	17
b. Surface codes	18
11. FT pseudo thresholds for ExtLEM and SALEM	21

### 1. Logical error channels

Let  $C = G_V \cdots G_1$  denote a faulty error-corrected quantum circuit, comprised of faulty error-corrected logical gates  $G_j$ , each including gadgets implementing logical gates, as well as syndrome measurements, decoding and recovery. We consider realistic ‘circuit-level’ noise models, where each physical operation in  $G_j$  carries a physical error (or ‘fault’) channel, with infidelity  $\epsilon$ . Fault channels are commonly assumed to be Pauli channels, which may be justified by Pauli-twirling. In the absence of faults, each  $G_j$  implements a logical gate  $g_j$  on the code space, such that  $G_{j,ideal}|c\rangle\rangle = g_j|c\rangle\rangle$ , where  $|c\rangle\rangle$  denotes (here and below) any code state.  $G_{j,ideal}$  differs from  $g_j$  in that while  $g_j$  acts only on the code space,  $G_{j,ideal}$  acts on any state and is guaranteed to map any state into the code space. Our goal is to obtain logical error channels  $\Lambda_L^{(j)}$  such that

$$\langle\langle O|C|c\rangle\rangle = \langle\langle O| \Lambda_L^{(V)} g_V \cdots \Lambda_L^{(1)} g_1 |c\rangle\rangle, \quad (3)$$

for any logical operator  $O$ . This is a purely logical description of the faulty circuit  $C$ , involving ideal logical gates followed by logical error channels. Equation (3) is the encoded version of the analogous equation for the original circuit and its physical errors. Such logical channels can then be targeted with LEM protocols, in order to reproduce expectation values in the ideal circuit.

Properly defining and estimating the channels  $\Lambda_L^{(j)}$  is subtle, because logical errors after  $G_j$  are due to combinations of (i) internal faults within  $G_j$ , and (ii) faults within earlier gates, that were not corrected, but did not lead to logical errors before  $G_j$ . The effect of the latter

can be represented as a physical input error channel  $\Lambda_{in}^{(j)}$ . The combined effect of input errors and faults in  $G_j$  leads to a physical output error channel  $\Lambda_{out}^{(j)}$ , such that

$$G_j \Lambda_{in}^{(j)} |c\rangle\rangle = \Lambda_{out}^{(j)} g_j |c\rangle\rangle. \quad (4)$$

We define the logical error channel  $\Lambda_L^{(j)}$  using the ideal version of the *next* gate  $G_{j+1}$ , such that

$$G_{j+1,ideal} \Lambda_{out}^{(j)} |c\rangle\rangle = g_{j+1} \Lambda_L^{(j)} |c\rangle\rangle. \quad (5)$$

This relies on the fact that  $G_{j+1,ideal}$  maps any input state to the code space. We then define the input to  $G_{j+1}$  as

$$\Lambda_{in}^{(j+1)} := \Lambda_{out}^{(j)} (\Lambda_L^{(j)})^{-1}. \quad (6)$$

Plugging Eq. (6) into Eq. (4) we get:

$$G_j \Lambda_{in}^{(j)} |c\rangle\rangle = \Lambda_{in}^{(j+1)} \Lambda_L^{(j)} g_j |c\rangle\rangle. \quad (7)$$

Assuming the first gate has no input errors,  $\Lambda_{in}^{(1)} = I$ ,<sup>1</sup> this gives an iterative definition of the input, output and logical error channels:

$$\Lambda_{in}^{(j)} \xrightarrow{\text{Eq. (4)}} \Lambda_{out}^{(j)} \xrightarrow{\text{Eq. (5)}} \Lambda_L^{(j)} \xrightarrow{\text{Eq. (6)}} \Lambda_{in}^{(j+1)} \quad (8)$$

The logical error channels can be shown by induction to satisfy

$$G_j \cdots G_1 |c\rangle\rangle = \Lambda_{in}^{(j+1)} \Lambda_L^{(j)} g_j \cdots \Lambda_L^{(1)} g_1 |c\rangle\rangle, \quad (9)$$

for all  $j < V$  (see Fig. 4).  $\Lambda_{in}^{(V)}$  and  $\Lambda_{out}^{(V)}$  are also defined by the iterative definition of Eq. (8), however, noting that  $\langle\langle O|$  produces a classical logical output, we define the final logical channel  $\Lambda_L^{(V)}$  through  $\langle\langle O| \Lambda_{out}^{(V)} |c\rangle\rangle = \langle\langle O| \Lambda_L^{(V)} |c\rangle\rangle$ , such that Eq. (3) holds exactly.

<sup>1</sup> Practically, the first gate corresponds to an error-corrected logical state preparation,  $G_1|c\rangle\rangle = |\text{prep. } c\rangle\rangle$ , which has no input state, but we choose to indicate the logical state explicitly in our notation. Similarly, the last gate corresponds to an error-corrected logical measurement,  $\langle\langle O| G_V = \langle\langle \text{meas. } O|$ , whose output is logical and classical.

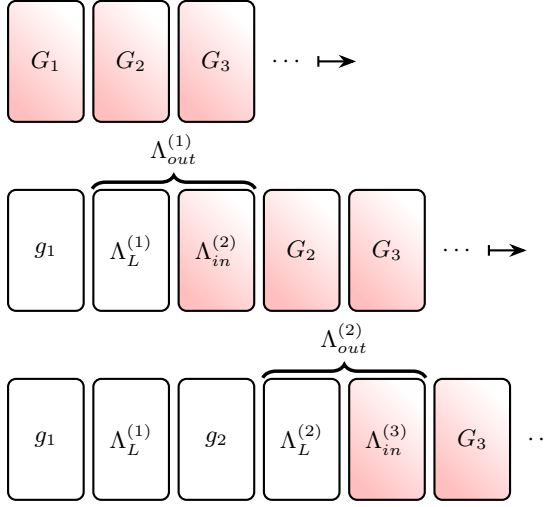


FIG. 4. The iterative construction of logical error channels from physical error channels. The scheme shows how by using Eq. (7) iteratively, the physical channels are replaced by logical channels and a fully logical description is reached in Eq. (9). Reddish blocks denote physical operations acting on the full physical Hilbert space, while white (unshaded) blocks denote logical operations restricted to code subspace.

This construction can be generalized to produce syndrome-conditioned logical error channel  $\Lambda_{L|s}^{(j)}$ , for each  $s = (s_j)_j$  a ‘global syndrome’. We note that for the sake of simplicity, we somewhat abuse notation: the  $s$  in the notation  $\Lambda_{L|s}^{(j)}$  involves only local syndromes from gates  $i = 1, \dots, j+1$ , since only these gates are involved in the iterative construction of  $\Lambda_L^{(j)}$  through Eq. (4)-(7). This can be indicated explicitly by writing  $\Lambda_{L|s_{1:j+1}}^{(j)}$ . One may condition only over the past local syndromes,  $s_1, \dots, s_j$ , to obtain a channel  $\Lambda_{L|s_{1:j}}^{(j)}$ , corresponding to a channel which is averaged over the future syndrome  $s_{j+1}$ . However, whether or not this may be done depends on how the resulting logical error channel is to be used, namely, on the exact LEM protocol. If the logical channel for  $G_j$ , namely  $\Lambda_L^{(j)}$  is to be used before  $s_{j+1}$  has been measured, it may be appropriate to average over  $s_{j+1}$ , and this is the case for FG-SALEM based on QP distributions (Appendix 4). However, when rejection is allowed, namely, in the context of CG-SALEM, this rejection imposes an a-priori known constraint on  $s_{j+1}$ , making it necessary to average only over *accepted* future syndromes  $s_{j+1}$ , see Appendix 10 a.

Collecting all local channels defines a ‘global logical error channel’  $\Lambda_{L|s} = (\Lambda_{L|s}^{(j)})_j$ , with (entry-wise) inverse  $\Lambda_{L|s}^{-1} = ((\Lambda_{L|s}^{(j)})^{-1})_j$ . Denoting the circuit volume (number of gates in  $C$ ) by  $V$ , we define the average syndrome-conditioned error rate by  $\epsilon_{L|s} = V^{-1} \sum_j \epsilon_{L|s}^{(j)}$ , where  $\epsilon_{L|s}^{(j)}$  is the infidelity of  $\Lambda_{L|s}^{(j)}$ . Given a partition  $S^{(j)} = \bigcup_k S_k^{(j)}$  of the syndromes in each gate, and a global

index  $\mathbf{k} = (k^{(j)})_j$ , the global subset-conditioned channel  $\Lambda_{L,\mathbf{k}}$  can be obtained in the same manner.

## 2. Temporally-local approximate logical error-channels

A downside of the construction of the logical error channels of Appendix 1 is that it is non-local in time, in the sense that  $\Lambda_L^{(j)}$  depends on all gates  $G_i$  with  $i = 1, \dots, j+1$ . We would like the logical channel to be more temporally-local, and easier to compute. Fortunately, at leading order, the temporal non-locality in the definition of  $\Lambda_L^{(j)}$  can be relaxed.

We define an approximate version of the logical error channel  $\Lambda_L^{(j)}$ , that depends only on  $G_{j-1}$ ,  $G_j$  and  $G_{j+1,ideal}$ . To this end we assume that each  $G_j$  is ‘ $t$ -fault-tolerant’ ( $t$ -FT), such that any combination of a weight  $w_{in}$  input error and  $w_f$  internal faults, with  $w_{in} + w_f \leq t$ , implies a weight  $w_{out} \leq w_f$  output error [2, 77, 78].

**Lemma 1 (Implications of  $t$ -fault-tolerance)**  $t$ -FT implies: (i) Input errors with weight  $\leq t$  are corrected in the absence of internal faults. (ii) Any combination of an input error and faults with  $w_{in} + w_f \leq t$  is either corrected, or ‘correctable’ - it will be corrected by the next logical gate, if no faults occur within it. (iii) If the number of faults in all pairs of consecutive logical gates  $G_j G_{j+1}$  is at most  $t$ , then the above two facts imply by induction that there is no logical error in the final state [5]. (iv) Leading-order logical errors are  $O(\epsilon^{t+1})$  and are due to fault-paths containing  $t+1$  faults in two consecutive gates  $G_j G_{j-1}$ .

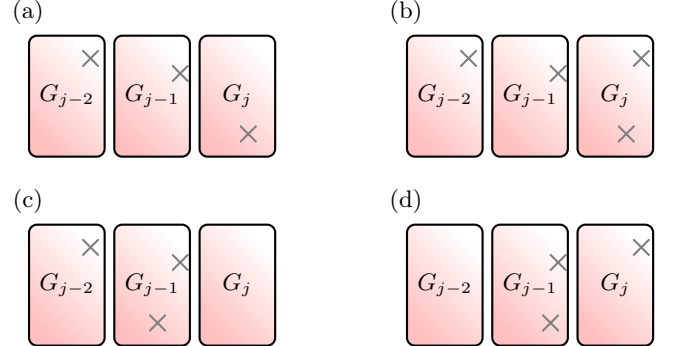


FIG. 5. Intuition for Lemma 1 and Proposition 1 with  $t = 2$ . Each panel shows three consecutive gates, with faults marked by  $\times$ 's. (a) The 2-FT property implies at most one output error after  $G_{j-1}$ , so the additional fault in  $G_j$  is not enough to cause a logical error. (b)  $G_j$  has at most one input error and two faults, so a logical error after  $G_j$  can occur. However this is a sub-leading weight-4 fault-path. (c) A leading order logical error may occur after  $G_{j-1}$ , but is included in the approximate logical channel of  $G_{j-1}$ , not of  $G_j$ . (d) A potential leading order logical error after  $G_j$ .

Using the above facts, we define an approximate logical channel  $\tilde{\Lambda}_L^{(j)}$  which is temporally-local, as sketched in Algorithm 1. We refer to this procedure as ‘physical-to-logical characterization’ (P2LC), since logical error channels are obtained from (characterized) physical error channels through classical simulation, as opposed to a direct ‘external’ characterization of logical gates [52, 53]. As opposed to external characterization, P2LC can characterize subset-conditioned logical channels efficiently. Moreover, the QPU time needed for external characterization scales as  $\epsilon_L^{-1}$ , which is exponential in the FT level  $t$ , while the QPU time for the physical characterization needed for P2LC scales as  $\epsilon^{-1}$ , with an additional polynomial dependence on  $t$ . P2LC is used in the simulations described in Appendix 10; a detailed account of the protocol, as well its required quantum and classical resources, can be found in Ref. [71].

---

**Algorithm 1** Physical-to-logical characterization (P2LC, sketch)

---

**Input:** A  $t$ -FT error-corrected circuit  $C = G_V \cdots G_1$ . A physical error model for faults occurring in each error-corrected logical gate  $G_j$ .

**Output:** An approximate logical error channel  $\tilde{\Lambda}_L^{(j)}$  for each gate  $G_j$ .

```

1: for  $j = 1$  to  $V$  do
2:   Replace  $\Lambda_{in}^{(j-1)}$  with  $\Lambda_{in}^{R,(j-1)} = I$ , and obtain  $\Lambda_{out}^{R,(j-1)}$  through Eq. (4).
3:   Extract  $\Lambda_c^{R,(j-1)}$ , the correctable part of  $\Lambda_{out}^{R,(j-1)}$ , by replacing each non-correctable Pauli in  $\Lambda_{out}^{R,(j-1)}$  by  $I$ .
4:   Replace  $\Lambda_{in}^{(j)}$  with  $\Lambda_{in}^{R,(j)} = \Lambda_c^{(j-1)}$ , and obtain  $\Lambda_{out}^{R,(j)}$  through Eq. (4).
5:   Replace  $\Lambda_{out}^{(j)}$  with  $\Lambda_{out}^{R,(j)}$ , and obtain  $\tilde{\Lambda}_L^{(j)}$  through Eq. (5).
6: end for
7: return  $\tilde{\Lambda}_L^{(1)}, \dots, \tilde{\Lambda}_L^{(V)}$ .

```

---

**Proposition 1 (Logical error channels are temporally-local at leading order)** *The approximate logical channel  $\tilde{\Lambda}_L^{(j)}$  depends only on the faulty gates  $G_{j-1}, G_j$ , and the ideal gate  $G_{j+1,ideal}$ ; and captures leading-order logical errors,  $\tilde{\Lambda}_L^{(j)} = \Lambda_L^{(j)} + O(\epsilon_L^{(j)}\epsilon)$ , where  $\epsilon_L^{(j)} = O(\epsilon^{t+1})$  is the infidelity of  $\Lambda_L^{(j)}$ .*

**Proof sketch:** Since leading order logical errors are due to weight- $(t+1)$  fault-paths contained in two consecutive logical gates  $G_j G_{j-1}$ , we can replace  $\Lambda_{in}^{(j-1)}$  with  $\Lambda_{in}^{R,(j-1)} = I$ , while causing an  $O(\epsilon^{t+2})$  change in  $\Lambda_L^{(j)}$ . We can therefore assume  $\Lambda_{in}^{(j-1)} = I$  for the sake of this proof, and, by Eq. (4) we may replace  $\Lambda_{out}^{(j-1)}$  with  $\Lambda_{out}^{R,(j-1)}$ , incurring an  $O(\epsilon^{t+2})$  error. Henceforth, we treat the two as interchangeable. Instead of Eq. (5) and (6) in the iterative definition, the algorithm now defines

$\Lambda_{in}^{R,(j)}$  as the correctable part  $\Lambda_c^{(j-1)}$  of  $\Lambda_{out}^{R,(j-1)}$ , and plugs it again in Eq. (4) to derive  $\Lambda_{out}^{R,(j)}$ , and from it  $\tilde{\Lambda}_L^{(j)}$  via Eq. (5) as illustrated in Fig. 6. Our remaining task is to show that the input channel defined in the original iterative procedure by  $\Lambda_{in}^{(j)} = \Lambda_{out}^{(j-1)}(\Lambda_L^{(j-1)})^{-1}$  (Eq. (6)) can be replaced by  $\Lambda_{in}^{R,(j)} = \Lambda_c^{(j-1)}$ , while modifying the resulting  $\Lambda_L^{(j)}$  by only  $O(\epsilon^{t+2})$ . Since  $\Lambda_L^{(j-1)} = I + O(\epsilon^{t+1})$  and  $\Lambda_{out}^{(j-1)} - \Lambda_c^{(j-1)} = O(\epsilon)$ , we have

$$\begin{aligned} \Lambda_{in}^{(j)} &= I + (\Lambda_{out}^{(j-1)} - \Lambda_L^{(j-1)})(\Lambda_L^{(j-1)})^{-1} & (10) \\ &= I + \Lambda_{out}^{(j-1)} - \Lambda_L^{(j-1)} + O(\epsilon^{t+2}). \end{aligned}$$

Writing  $\Lambda_{out}^{(j-1)}$  in terms of its correctable and non-correctable parts,  $(\Lambda_{out}^{(j-1)} - I) = (\Lambda_c^{(j-1)} - I) + (\Lambda_{nc}^{(j-1)} - I)$ , we find

$$\Lambda_{in}^{(j)} = \Lambda_c^{(j-1)} + (\Lambda_{nc}^{(j-1)} - \Lambda_L^{(j-1)}) + O(\epsilon^{t+2}). \quad (11)$$

The difference  $\Lambda_{nc}^{(j-1)} - \Lambda_L^{(j-1)}$  is  $O(\epsilon^{t+1})$  (because each one of the channels is  $I + O(\epsilon^{t+1})$  by itself) and vanishes under  $G_{j,ideal}$ , so, combined with  $G_j = G_{j,ideal} + O(\epsilon)$ , we find

$$G_j(\Lambda_{nc}^{(j-1)} - \Lambda_L^{(j-1)}) = O(\epsilon^{t+2}). \quad (12)$$

Thus,

$$G_j \Lambda_{in}^{(j)} = G_j \Lambda_c^{(j-1)} + O(\epsilon^{t+2}), \quad (13)$$

showing that replacing  $\Lambda_{in}^{(j)}$  with  $\Lambda_c^{(j-1)}$  in Eq. (4) can only modify  $\Lambda_{out}^{(j)}$ , by  $O(\epsilon^{t+2})$ ; plugging this into Eq. (5) we get that  $\Lambda_L^{(j)}$  is also changed by  $O(\epsilon^{t+2})$ , deriving Prop. 1.

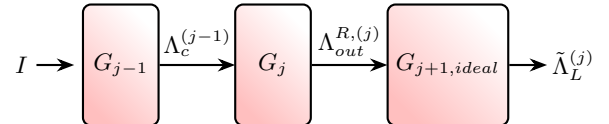


FIG. 6. Computation of  $\tilde{\Lambda}_L^{(j)}$  in Algorithm 1. The channel  $\Lambda_{in}^{(j-1)}$  is replaced with  $\Lambda_{in}^{R,(j-1)} = I$  and serves as input for  $G_{j-1}$  to obtain  $\Lambda_{out}^{R,(j-1)}$  using Eq. (4). Non correctable errors of  $\Lambda_{out}^{R,(j-1)}$  are replaced by  $I$  to obtain  $\Lambda_c^{(j-1)}$ . Using Eq. (4) again,  $\Lambda_c^{(j-1)}$  serves as the input channel to  $G_j$ , resulting in  $\Lambda_{out}^{R,(j)}$ . Finally,  $G_{j+1,ideal}$  is applied to obtain  $\tilde{\Lambda}_L^{(j)}$  using Eq. (5).

Algorithm 1 generalizes to the syndrome-conditioned case, giving a channel  $\tilde{\Lambda}_{L|s_{j-1:j+1}}^{(j)}$ , that agrees with  $\Lambda_{L|s}^{(j)}$  to leading order in  $\epsilon$ :

$$\tilde{\Lambda}_{L|s_{j-1:j+1}}^{(j)} = \Lambda_{L|s}^{(j)} + O(\epsilon_{L|s}^{(j)}\epsilon). \quad (14)$$

This generalizes Prop. 1 to syndrome-conditioned logical channels. The proof follows similar lines.

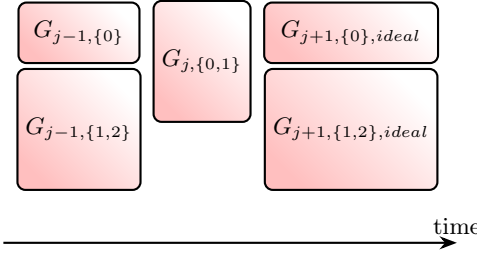


FIG. 7. Illustration of a one-step past and future light-cones required to compute the leading order logical error channel of a gate in layer  $j$  acting on logical qubits  $\{0, 1\}$ . It suffices to simulate this local environment in order to obtain the leading-order logical error channel  $\tilde{\Lambda}_L^{(j, \{0, 1\})}$ .

Note that our approximate construction assumed that each gate  $G_j$  is  $t$ -FT as an operation on all logical qubits in the circuit  $C$ . Assume now that  $G_j = \otimes_\alpha G_{j,\alpha}$  is a layer of  $t$ -FT gates  $G_{j,\alpha}$  acting on non-overlapping subsets  $Q_\alpha$  of logical qubits. In this case we can similarly obtain, for each  $G_{j,\alpha}$ , an approximate space-time-local logical error channel  $\tilde{\Lambda}_L^{(j,\alpha)}$  acting on  $Q_\alpha$ , and which depends only on the gates  $G_{j-1,\alpha'}$  with overlapping support  $Q_\alpha \cap Q'_{\alpha'} \neq \emptyset$  (the ‘one-step past light-cone’), and the ideal gates  $G_{j+1,\alpha',ideal}$  with overlapping support (the ‘one-step future light-cone’), see Fig. 7. Accordingly,  $\tilde{\Lambda}_L^{(j,\alpha)}$  may be conditioned on syndromes in these near-by gates.

### 3. Fine-grained SALEM

An FG-SALEM protocol can be specified by a mapping of global syndromes to corresponding EM protocols and weights,

$$FG\text{-SALEM} : \mathbf{s} \mapsto (EM_{\mathbf{s}}, w_{\mathbf{s}}). \quad (15)$$

The EM protocol  $EM_{\mathbf{s}}$  is applied to shots in which the syndrome  $\mathbf{s}$  is measured, resulting in a ‘mitigated outcome’  $o$ . Applying this process for  $N$  shots in which  $M \leq N$  distinct syndromes  $\mathbf{s}_1, \dots, \mathbf{s}_M$  are measured, results in  $M$  corresponding mitigated outcomes  $o_1, \dots, o_M$ . These are combined to an  $N$ -shot SALEM estimator by averaging with the weights  $w_{\mathbf{s}}$ ,

$$\bar{o} = \frac{w_{\mathbf{s}_1} o_{\mathbf{s}_1} + \dots + w_{\mathbf{s}_M} o_{\mathbf{s}_M}}{w_{\mathbf{s}_1} + \dots + w_{\mathbf{s}_M}}. \quad (16)$$

The protocol  $EM_{\mathbf{s}}$  is designed to invert the effect of  $\Lambda_{L|\mathbf{s}}$  on the ideal expectation value  $\langle O \rangle$  of an operator  $O$  measured at the end of  $C$ . Since the inverse  $\Lambda_{L|\mathbf{s}}^{-1}$  is generally not a physical operation that can be implemented within a single shot, the protocols  $EM_{\mathbf{s}}$  are meant to ‘implement’  $\Lambda_{L|\mathbf{s}}^{-1}$  only in expectation, such that, conditioned on any measured syndrome  $\mathbf{s}$ , the expectation of the mitigated outcome  $o$  reproduces the ideal expectation value,

$$\mathbb{E}[o_{\mathbf{s}}] = \mathbb{E}[o|\mathbf{s}] = \langle O \rangle. \quad (17)$$

This requirement may be relaxed to enable a small bias  $b_{\mathbf{s}} = \mathbb{E}[o_{\mathbf{s}}] - \langle O \rangle$ , such that  $|b_{\mathbf{s}}| \ll V\epsilon_{L|\mathbf{s}}$ .

Operationally, each protocol  $EM_{\mathbf{s}}$  involves modifications to the given circuit  $C$ , as well as a post-processing of the outcomes of measuring  $O$  at the end of the resulting modified circuits. Some of these circuit modifications may be  $\mathbf{s}$ -independent, shared by all protocols  $EM_{\mathbf{s}}$ , and performed prior to circuit execution, as in standard EM and in ExtLEM. However, some circuit modifications may be  $\mathbf{s}$ -dependent, and must therefore be performed as adaptive logic during circuit execution, after the relevant part of the global syndrome  $\mathbf{s}$  is measured, in analogy with the recovery operation of EC.

Given Eq. (17), the law of total expectation implies that  $\bar{o}$  is unbiased,  $\mathbb{E}[\bar{o}] = \mathbb{E}[\mathbb{E}[o|\mathbf{s}]] = \langle O \rangle$ , for any choice of weights  $w_{\mathbf{s}}$ , which can be chosen to minimize the variance  $\mathbb{V}[\bar{o}]$ . We assume upper bounds  $\Gamma_{\mathbf{s}}$  for the shot overheads of the EM protocols  $EM_{\mathbf{s}}$  are known, such that

$$\mathbb{V}[o_{\mathbf{s}}] = \mathbb{V}[o|\mathbf{s}, N_{\mathbf{s}}] \leq \Gamma_{\mathbf{s}}/N_{\mathbf{s}}. \quad (18)$$

Here,  $N_{\mathbf{s}}$  is the number of shots in which a syndrome  $\mathbf{s}$  was measured among the  $N$  shots used to generate  $\bar{o}$ .

Given the bounds  $\Gamma_{\mathbf{s}}$ , we prove:

**Theorem 1 (Shot overhead of FG-SALEM)** *Let  $\bar{o}$  be an  $N$ -shot FG-SALEM estimator (Eq. (16)) based on unbiased EM protocols  $EM_{\mathbf{s}}$  (Eq. (17)), with shot overheads upper bounded by  $\Gamma_{\mathbf{s}}$  (Eq. (18)). Then, the corresponding upper bound on  $\mathbb{V}[\bar{o}]$  is minimized by the ‘inverse-variance’ (IV) weights  $w_{\mathbf{s}} = N_{\mathbf{s}}/\Gamma_{\mathbf{s}}$ . The optimal bound is given by  $\mathbb{V}[\bar{o}] \leq \mathbb{H}[\Gamma_{\mathbf{s}}]/N + O(1/N^2)$ , where  $\mathbb{H}[\Gamma_{\mathbf{s}}] = (\mathbb{E}[\Gamma_{\mathbf{s}}^{-1}])^{-1}$  is the ‘harmonic expectation’ of  $\Gamma_{\mathbf{s}}$  over global syndromes  $\mathbf{s}$ . Thus, the shot overhead for FG-SALEM with IV weights is bounded by*

$$\Gamma_{SALEM}^{FG} = \mathbb{H}[\Gamma_{\mathbf{s}}], \quad (19)$$

up to negligible  $O(1/N)$  corrections.

### 4. FG-SALEM with QP distributions

The protocols  $EM_{\mathbf{s}}$  may be based on quasi-probability (QP) distributions  $q_{\sigma|s_{1:j}}^{(j)} \in \mathbb{R}$ ,  $\sum_{\sigma} q_{\sigma|s_{1:j}}^{(j)} = 1$ , depending on  $s_{1:j} = (s_1, \dots, s_j)$ , such that

$$(\Lambda_{L|s_{1:j}}^{(j)})^{-1} = \sum_{\sigma} q_{\sigma|s_{1:j}}^{(j)} \sigma, \quad (20)$$

where  $\Lambda_{L|s_{1:j}}^{(j)}$  is the exact logical error channel of the logical gate  $G_j$ . Writing  $q_{\sigma|s_{1:j}}^{(j)} = W_{s_{1:j}}^{(j)} \mathbf{s}_{\sigma|s_{1:j}}^{(j)} p_{\sigma|s_{1:j}}^{(j)}$ , with the ‘QP norm’  $W_{s_{1:j}}^{(j)} = \sum_{\sigma} |q_{\sigma|s_{1:j}}^{(j)}|$  and signs  $\mathbf{s}_{\sigma|s_{1:j}}^{(j)} = \text{sign}(q_{\sigma|s_{1:j}}^{(j)})$ , local inversion can be implemented (in expectation) by the following procedure. (i) For each shot and each  $j = 1, \dots, V$ , apply  $G_j$  and obtain a new syndrome  $s_j$ ; then apply the operation  $\sigma$  with probability  $p_{\sigma|s_{1:j}}^{(j)}$  (this is an  $\mathbf{s}$ -dependent circuit modification).

(ii) Measure  $O$  at the end of the circuit and multiply the outcome by the products  $W_s = \prod_{j=1}^V W_{s_{1:j}}^{(j)}$  and  $s_s = \prod_{j=1}^V s_{\sigma|s_{1:j}}^{(j)}$ ; then average over shots in which the same  $s$  was observed to obtain  $o_s$ . Thus, FG-SALEM based on QPs can be understood as adding to the deterministic recovery  $s_{1:j} \mapsto R_{s_{1:j}}$  of EC a quasi-probabilistic recovery:  $s_{1:j} \mapsto \sigma$  with quasi-probability  $q_{\sigma|s_{1:j}}^{(j)}$ . As discussed in Sec. IV, this can be viewed as including a deterministic correction of  $R_{s_{1:j}}$  to the optimal ML recovery. We can similarly work with the approximate channels  $\tilde{\Lambda}_{L|s_{j-1:j}}^{(j)}$ .

**Theorem 2 (Conditioned local inversion is unbiased)** *Local inversion based on the exact logical error channels  $\Lambda_{L|s_{1:j}}^{(j)}$  defined in Appendix 1 satisfies Eq. (17). Using the approximate channels  $\tilde{\Lambda}_{L|s_{j-1:j}}^{(j)}$  leads to a small bias  $b_s = O(V\epsilon_{L|s}) \ll V\epsilon_{L|s}$ .*

Using the simple bounds  $\Gamma_s = W_s^2$  we find

$$\Gamma_{SALEM}^{FG} = \mathbb{H}[W_s^2]. \quad (21)$$

If the input channel to gate  $G_j$  is independent of past syndromes, we can write  $W_s = \prod_{j=1}^V W_{s_j}^{(j)}$ , where  $W_{s_j}^{(j)}$  are independent as random variables. In this case

$$\Gamma_{SALEM}^{FG} = \prod_j \mathbb{H}[(W_{s_j}^{(j)})^2]. \quad (22)$$

## 5. Advantage of FG-SALEM over ExtLEM

We can now compare the shot overhead of FG-SALEM to that of ExtLEM. To make a ‘fair’ comparison, we assume that both ExtLEM and FG-SALEM are based on the same underlying EM protocol, which satisfies a functional relation  $\Gamma = f(\epsilon)$  between the infidelity  $\epsilon$  of the mitigated error channel (averaged over all gates in the circuit), and a corresponding bound  $\Gamma$  on the shot overhead. Thus, the shot overhead for ExtLEM is bounded by  $\Gamma_{ExtLEM} = f(\epsilon_L)$ , and the shot overhead bounds for FG-SALEM are  $\Gamma_s = f(\epsilon_{L|s})$ . Note that  $\epsilon_L = \mathbb{E}[\epsilon_{L|s}]$ .

**Theorem 3 (Advantage of FG-SALEM over ExtLEM in shot overhead)** *Let  $\Gamma_{ExtLEM} = f(\epsilon_L)$  be a bound on the shot overhead of ExtLEM based on a given EM protocol, as a function of the (gate-averaged) logical error rate  $\epsilon_L$ . Assume that  $f$  is monotonically increasing and convex, and that  $f(0) = 1$ . Consider FG-SALEM based on the same given EM protocol, with overhead bounds  $\Gamma_s = f(\epsilon_{L|s})$  and corresponding IV weights. Then the shot overhead of FG-SALEM can only be lower than that of ExtLEM, due to a ‘generalized mean inequality’,*

$$\Gamma_{SALEM}^{FG} = \mathbb{H}[\Gamma_s] \leq (f \circ \mathbb{E} \circ f^{(-1)})[\Gamma_s] = \Gamma_{ExtLEM}, \quad (23)$$

where  $f^{(-1)}$  the inverse function of  $f$ , and  $\circ$  denotes the composition of functions. An equality  $\Gamma_{SALEM}^{FG} = \Gamma_{ExtLEM}$  occurs if the syndrome-conditioned logical infidelity is uniform,  $\epsilon_{L|s} = \epsilon_L$ , leading to a uniform  $\Gamma_s$ . Assuming  $f(\epsilon)$  does not happen to be of the form  $1/(1 - c\epsilon)$  with some  $c \geq 0$ , an equality  $\Gamma_{SALEM}^{FG} = \Gamma_{ExtLEM}$  occurs only if  $\epsilon_{L|s}$  is uniform.

The conditioned infidelity  $\epsilon_{L|s}$  is generically highly non-uniform, leading to a significantly reduced shot overhead in FG-SALEM.

**Example 1 (Exponential shot overhead)** *As discussed in the main text, a simplified but representative expression for the shot overhead in EM protocols is given by  $f(\epsilon) = e^{\lambda V \epsilon}$ , where  $V$  is the circuit volume and  $\lambda$  is an order-1 coefficient that may be referred to as the ‘blowup rate’, and that depends on the details of the EM protocol. Note that  $f$  is monotonically increasing and convex, with  $f(0) = 1$ . In this case*

$$\Gamma_{ExtLEM} = (f \circ \mathbb{E} \circ f^{(-1)})[\Gamma_s] = \exp(\mathbb{E}[\log \Gamma_s]) = \mathbb{G}[\Gamma_s], \quad (24)$$

where  $\mathbb{G}$  denotes the ‘geometric expectation’. The well known GM-HM inequality then shows directly that

$$\Gamma_{SALEM}^{FG} = \mathbb{H}[\Gamma_s] \leq \mathbb{G}[\Gamma_s] = \Gamma_{ExtLEM}, \quad (25)$$

in accordance with Theorem 3.

The assumptions in Theorem 3 can be weakened:  $\Gamma_{SALEM}^{FG} \leq \Gamma_{ExtLEM}$  holds for more general functional relations  $\Gamma_s = f(\Lambda_{L|s})$ , under the weaker requirement that the reciprocal  $1/f$  is convex over the relevant space of channels  $\Lambda$  (e.g., the space of tuples of Pauli channels). This convexity requirement can be further relaxed if  $f(\Lambda_{L|s}) = \prod_{j=1}^V g(\Lambda_{L|s^{(j)}}^{(j)})$  is a product of local overheads  $\Gamma_{s^{(j)}}^{(j)} = g(\Lambda_{L|s^{(j)}}^{(j)})$ , corresponding to individual logical gates. This is the case in e.g., Example 1 and Eq. (22). In this case,

$$\Gamma_{SALEM}^{FG} = \prod_{j=1}^V \mathbb{H}[\Gamma_{s^{(j)}}^{(j)}] \quad (26)$$

is explicitly exponential in  $V$ . However, the advantage over ExtLEM is also exponential in  $V$ , as quantified by the blowup rates  $\lambda_{SALEM}^{FG} = (\epsilon_L V)^{-1} \log \Gamma_{SALEM}^{FG}$  and  $\lambda_{ExtLEM} = (\epsilon_L V)^{-1} \log \Gamma_{ExtLEM}$ , both defined in the limit  $\epsilon_L \rightarrow 0$ . Assuming FG-SALEM and ExtLEM are based on an EM protocol with blowup rate  $\lambda$ , such that  $g(\Lambda) = 1 + \lambda\epsilon + O(\epsilon^2)$  (where  $\epsilon$  is the infidelity of  $\Lambda$ ), it is clear that  $\lambda_{ExtLEM} = \lambda$ . However, under the requirement  $1/g(\Lambda) \geq 1 - \lambda\epsilon$ , which is weaker than convexity of  $1/g$  and always holds for  $\epsilon > \lambda^{-1}$ , we find

$$\begin{aligned} \lambda_{SALEM}^{FG} &= - \lim_{\epsilon_L \rightarrow 0} \epsilon_L^{-1} \log \mathbb{E}[1/g(\Lambda_{L|s})] \quad (27) \\ &\leq - \lim_{\epsilon_L \rightarrow 0} \epsilon_L^{-1} \log \mathbb{E}[1 - \lambda\epsilon_{L|s}] \\ &= - \lim_{\epsilon_L \rightarrow 0} \epsilon_L^{-1} \log(1 - \lambda\epsilon_L) = \lambda, \end{aligned}$$

with the gap given by  $\lambda - \lambda_{SALEM}^{FG} = \epsilon_L^{-1} \mathbb{E}[1/g(\Lambda_{L|s}) - 1 + \lambda \epsilon_{L|s}] + O(\epsilon_L)$ .

## 6. CG-SALEM

The following corollary of Theorems 1-3 describes the shot overhead increase in SALEM due to both coarse-graining and rejection.

**Corollary 1 (Shot overhead of coarse-grained SALEM)** *In analogy with Theorem 1, the shot overhead of SALEM with the partition  $\{S_k\}$  of global syndromes and IV weights is given by  $\Gamma_{SALEM}^{\{S_k\}} = \mathbb{H}[\Gamma_k]$ . Under the assumptions of Theorem 3 (or any of its generalizations),*

$$\Gamma_{SALEM}^{FG} \leq \Gamma_{SALEM}^{\{S_k\}} \leq \Gamma_{ExtLEM}. \quad (28)$$

Moreover, rejecting a subset  $S_{Rej} \in \{S_k\}$  further increases the shot overhead to

$$\Gamma_{SALEM}^{\{S_k\}, Rej} = \mathbb{P}_{Acc}^{-1} \mathbb{H}[\Gamma_k | Acc] \geq \Gamma_{SALEM}^{\{S_k\}}, \quad (29)$$

where  $\mathbb{P}_{Acc} = 1 - \mathbb{P}(S_{Rej})$  is the acceptance probability. An equality occurs if and only if  $\Gamma_s = \infty$  for all  $s \in S_{Rej}$ , or  $\mathbb{P}_{Acc} = 1$ .

Note that the increase in shot overhead due to coarse-graining would be mild if  $\Gamma_s$  are relatively uniform *within* each subset  $S_k$ , with significant variations only *between* subsets. The shot overhead increase due to rejection would be mild if  $\Gamma_k \gg \Gamma_{k'}$  for all rejected  $k$  and accepted  $k'$ .

## 7. Violation and derivation of lower bounds for shot overheads in LEM

Known lower bounds on the shot overhead of physical EM do not hold for error-corrected circuits, which involve adaptive operations [47–50]. However, it is clear that these bounds do hold for ExtLEM, which mitigates  $\Lambda_L$  while ignoring syndrome data. As an example, if  $\Lambda_L$  takes the form of a layer of single-qubit depolarizing channels, we get

$$\Gamma_{ExtLEM} \geq f_{bound}(\Lambda_L), \quad (30)$$

where  $f_{bound}(\Lambda_L) = (1 - 4\epsilon_L/3)^{-2D}$ , and  $D$  is the circuit depth [48, 49]. Generalization to more general logical error channels is done by replacing  $(1 - 4\epsilon/3)^2$  by an appropriate ‘contraction factor’, see Appendix I in [48] and the parameter  $\gamma^2$  in [49]. For a layer of bit-flip channels,  $f_{bound}(\Lambda) = (1 - 2\epsilon)^{-2D}$ . For a general layer of single-qubit Pauli channels  $\Lambda = (1 - \epsilon)I + \epsilon(q_X X + q_Y Y + q_Z Z)$ ,  $f_{bound}(\Lambda) = |1 - 2\epsilon \min_{i \neq j} (q_i + q_j)|^{-2D}$ .

SALEM’s use of syndrome data implies that the same lower bound does not hold for the SALEM estimator  $\bar{o}$

(Eq. (16)). But it does hold for each  $o_k = o|k, N_k$ , giving  $\Gamma_k \geq f_{bound}(\epsilon_{L|k})$ . This implies a lower bound

$$\Gamma_{SALEM} = \mathbb{H}[\Gamma_k] \geq \mathbb{H}[f_{bound}(\Lambda_{L|k})]. \quad (31)$$

As in Appendix 3, we can ensure that the SALEM bound is less restrictive than that of ExtLEM when  $1/f_{bound}$  is convex:

$$\mathbb{H}[f_{bound}(\Lambda_{L|k})] \leq f_{bound}(\Lambda_L). \quad (32)$$

This happens e.g., in the depolarizing and bit-flip cases (and more generally when some  $q_i = 0$ ). For layers of general single-qubit Pauli channels,  $1/f_{bound}$  is convex if  $\epsilon < 3/4$ , and violates convexity very mildly otherwise. We note that the use of ML decoding ensures that the probability for the identity is larger (or equal) to that of non-identity Paulis, which implies  $\epsilon < 3/4$ .

The same approach can be applied to obtain tighter lower bounds for SALEM and ExtLEM based on specific EM protocols, such as Eq. (34) (which satisfies our convexity requirement).

To summarize, we find that SALEM can break lower bounds that hold for physical EM and ExtLEM with any EM protocol. However, these lower bounds can be used to derive weaker lower bounds (Eq. (31)) that do hold for SALEM.

An interesting open question is whether SALEM is the optimal LEM scheme based on syndrome data. E.g., does the lower bound  $\mathbb{H}[f_{bound}(\epsilon_{L|s})]$  hold for any LEM protocol that makes use of syndrome data?

## 8. Case study: Binary CG-SALEM with QP distributions

As discussed in the main text, binary partitions are useful within CG-SALEM since they reduce and even eliminate the implementation challenges of finer partitions. Moreover, the binary case allows for an analytic computation of the blowup rate for CG-SALEM as a function of simple quantities, providing intuition for the results presented in Appendices 3–6 and in the main text.

To analytically compute the blowup-rate for binary CG-SALEM, we start with Eq. (26), and assume (i) a uniform circuit, where all gates are equal, and (ii) a binary coarse graining of local syndromes  $S = S_0 \cup S_1$ , such that

$$\Gamma_{SALEM}^{\{S_0, S_1\}} = (\mathbb{H}[\Gamma_k])^V. \quad (33)$$

Here,  $k = 0, 1$ , and  $\Gamma_k$  is the shot overhead for mitigating the channel  $\Lambda_{L|k}$ , satisfying  $\Gamma_k = g(\Lambda_{L|k})$ , for some function  $g$  with expansion  $g(\Lambda) = 1 + \lambda\epsilon + O(\epsilon^2)$ , where  $\epsilon$  is the infidelity of  $\Lambda$ .

We specifically consider QP distributions  $\Lambda_{L|k}^{-1} = \sum_{\sigma} q_{\sigma|k} \sigma$ , such that  $\Gamma_k = W^2(\Lambda_{L|k})$  is the square of the QP norm  $W(\Lambda_{L|k}) = \sum_{\sigma} |q_{\sigma|k}|$ . Assuming the mitigated

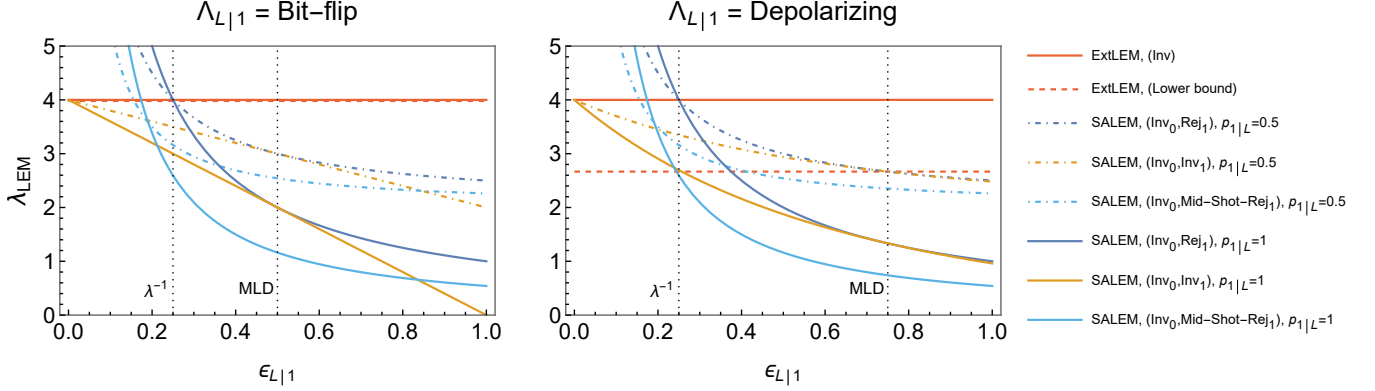


FIG. 8. Blowup rate  $\lambda_{LEM}$  for three versions of binary CG-SALEM, compared to that of ExtLEM (red). All protocols are based on a local inversion with QPs ('Inv'), and we include lower bounds that apply to any ExtLEM protocol (red, dashed), but can be violated by SALEM (see Appendix 7). Binary CG-SALEM is defined by a partition  $S = S_0 \cup S_1$  of local syndromes. We parameterize the blowup rates with  $\epsilon_{L|1} = \mathbb{P}(\text{logical error} | S_1)$  (x-axis) and  $p_{1|L} = \mathbb{P}(S_1 | \text{logical error})$  (dot-dashed vs. solid SALEM lines). The 'good' subset  $S_0$  is inverted, while the 'bad' subset  $S_1$  is rejected (Rej<sub>1</sub>, blue), inverted (Inv<sub>1</sub>, orange), or rejected mid-shot (Mid-Shot-Rej<sub>1</sub>, cyan). For mid-shot rejection, we assume a circuit volume  $V = \epsilon_L^{-1}$ , see Appendix 9. Left panel:  $\Lambda_{L|1}$  is a bit-flip channel. Right:  $\Lambda_{L|1}$  is a (single-qubit) depolarizing channel. ExtLEM and binary CG-SALEM with rejection or mid-shot rejection are identical between left and right panels. Only the ExtLEM lower bound and Inv<sub>1</sub> depend on the details of  $\Lambda_{L|1}$ , beyond its infidelity  $\epsilon_{L|1}$ . Dotted vertical lines: The Rej<sub>1</sub> version of binary CG-SALEM improves over ExtLEM only if  $\epsilon_{L|1} > \lambda^{-1} = 1/4$ , and agrees with Inv<sub>1</sub> when  $\Lambda_{L|1}$  is singular. For the bit-flip and depolarizing channels, this happens at the maximal  $\epsilon_{L|1}$  possible under ML decoding, at 1/2 and 3/4, respectively. Larger values of  $\epsilon_{L|1}$  correspond to decoding errors on  $S_1$ , which Inv<sub>1</sub> implicitly corrects without a shot overhead. This figure can be used to understand the numerical blowup rates in Fig. 3 in the main text, in light of the numerical values of  $\epsilon_{L|1}$  and  $p_{1|L}$  in that figure.

channel  $\Lambda$  is trace-preserving, one may obtain a lower bound on the norm of any QP distribution for  $\Lambda$  [41],

$$W^2(\Lambda) \geq \left( \frac{1+\epsilon}{1-\epsilon} \right)^2 = 1 + 4\epsilon + O(\epsilon^2). \quad (34)$$

It follows that the optimal blow-up rate for QPs is  $\lambda = 4$ . This is achieved by various known QP distributions, and we restrict attention to this 'blowup-optimal' case.

Assuming  $t$ -FT logical gates, we define the 'good' set  $S_0$  to include all syndromes which can be obtained due to a fault path with weight  $\leq t$  (and possibly some syndromes that can be obtained due to higher-weight fault-paths), and  $S_1$  to be the complementary 'bad' set. The probability for measuring a syndrome in  $S_1$  is  $p_1 = \mathbb{P}(s \in S_1) = O(\epsilon^{t+1})$ , where  $\epsilon$  is the physical infidelity. The assumption of  $t$ -FT implies  $\epsilon_L = O(\epsilon^{t+1})$ . Assuming that  $\epsilon_L = \Theta(\epsilon^{t+1})$ , so no 'accidental'  $(t+1)$ -FT occurs, we have  $p_1 = O(\epsilon_L)$ , and  $p_0 = 1 - O(\epsilon_L)$ . It follows that  $\epsilon_{L|0} = \mathbb{P}(\text{error} | s \in S_0) \leq \epsilon_L/p_0 = O(\epsilon_L)$ , and therefore  $\Gamma_0 = 1 - 4\epsilon_{L|0} + O(\epsilon_L^2)$ . Note however that  $\epsilon_{L|1} = \mathbb{P}(\text{error} | s \in S_1) \leq \epsilon_L/p_1$  need not be small, and may take any value in  $[0, 1]$ . Generically,  $\epsilon_{L|1}$  will not be small, since the leading contribution to  $S_1$  comes from weight- $(t+1)$  fault-paths.

It is useful to parametrize  $\lambda_{SALEM}^{\{S_0, S_1\}}$  as a function of  $\epsilon_{L|1}$  and  $p_{1|L} = \mathbb{P}(s \in S_1 | \text{error})$ , which is the fraction of logical errors contained in  $S_1$ . Note that  $p_1 = \epsilon_L p_{1|L} / \epsilon_{L|1}$  (Bayes' theorem), and  $\epsilon_L = \mathbb{E}[\epsilon_{L|k}] = p_0 \epsilon_{L|0} + p_1 \epsilon_{L|1}$ .

With these relations, we expand

$$\begin{aligned} & p_0 \Gamma_0^{-1} + p_1 \Gamma_1^{-1} \\ &= 1 - 4\epsilon_{L|0} - p_1(1 - \Gamma_1^{-1}) + O(\epsilon_L^2) \\ &= 1 - \epsilon_L \left( 4(1 - p_{1|L}) + \frac{1 - \Gamma_1^{-1}}{\epsilon_{L|1}} p_{1|L} \right) + O(\epsilon_L^2), \end{aligned} \quad (35)$$

implying

$$\begin{aligned} \lambda_{SALEM}^{\{S_0, S_1\}} &= \lim_{\epsilon_L \rightarrow 0} \epsilon_L^{-1} \log \mathbb{H}[\Gamma_k] \\ &= - \lim_{\epsilon_L \rightarrow 0} \epsilon_L^{-1} \log (p_0 \Gamma_0^{-1} + p_1 \Gamma_1^{-1}) \\ &= 4(1 - p_{1|L}) + \frac{1 - \Gamma_1^{-1}}{\epsilon_{L|1}} p_{1|L}. \end{aligned} \quad (36)$$

This can be understood as a weighted average of the blowup rate  $\lambda_0 = \lambda = 4$  for mitigating  $\Lambda_{L|0}$ , and the blowup rate  $\lambda_1 = (1 - \Gamma_1^{-1})\epsilon_{L|1}^{-1}$  for mitigating  $\Lambda_{L|1}$ ; with weights given by  $1 - p_{1|L}$  and  $p_{1|L}$ . As a special case of Eq. (27), an advantage over ExtLEM is obtained when

$$1/\Gamma_1 = W^{-2}(\Lambda_{L|1}) > 1 - 4\epsilon_{L|1}, \quad (37)$$

such that  $\lambda_1 < 4$ . The relation  $W^{-2}(\Lambda) > 1 - 4\epsilon$  holds for all (blowup-optimal) QP distributions we are aware of, implying that  $\lambda_{SALEM}^{\{S_0, S_1\}}$  is always better than  $\lambda_{ExtLEM} = \lambda = 4$ .

The blowup rate in case  $S_1$  is rejected is obtained in the limit  $\Gamma_1 \rightarrow \infty$ ,

$$\lambda_{SALEM}^{\{S_0, S_1\}, Rej} = 4(1 - p_{1|L}) + \epsilon_{L|1}^{-1} p_{1|L}, \quad (38)$$

which again can be understood as a weighted average of blowup rates, where now  $\lambda_1 = \epsilon_{L|1}^{-1}$  is the blowup due to rejection. In accordance with Corollary 1, rejection always increases the blowup rate, unless  $\Gamma_1 = \infty$ . An improvement over ExtLEM isn't guaranteed, and requires  $\epsilon_{L|1} > \lambda^{-1} = 1/4$ .

**Example 2** The squared QP norm  $W^2(\Lambda) = (1 - 2\epsilon)^{-2}$  gives a very simple expression,

$$\lambda_{SALEM}^{\{S_0, S_1\}} = 4(1 - p_{1|L}\epsilon_{L|1}). \quad (39)$$

This QP norm is obtained from a series expansion  $\Lambda^{-1} = \sum_{k=0}^{\infty} (I - \Lambda)^k$  which can be used to efficiently invert any Pauli channel  $\Lambda$  with  $\epsilon < 1/2$ . Moreover, the same QP norm is valid for all  $\epsilon \neq 1/2$  if  $\Lambda = (1 - \epsilon)I + \epsilon\sigma$  is a Pauli channel with a single Pauli error  $\sigma$ , since in this case we may use the QP distribution  $\Lambda^{-1} = |1 - 2\epsilon| \text{sgn}(1 - 2\epsilon) ((1 - \epsilon)I - \epsilon\sigma)$ . At  $\epsilon_{L|1} = 1/2$  the single-Pauli error channel isn't invertible, and the QP norm diverges. Note that  $W^2 = (1 - 2\epsilon)^{-2}$  is convex and monotonically increasing on  $[0, 1/2]$ , as required by Theorem 3, but not on  $[0, 1]$ . However,  $W^{-2}(\epsilon)$  is convex on  $[0, 1]$ , and in particular satisfies the weaker requirement  $W^{-2} > 1 - 4\epsilon$ .

For  $\epsilon_{L|1} > 1/2$  this example corresponds to a 'decoding error' on  $S_1$ , since, assuming the optimal ML decoder, the identity operator must have the highest probability in  $\Lambda_{L|1}$ . Accordingly, the overhead for inverting  $\Lambda_{L|1}$  decreases in the range  $1/2 < \epsilon_{L|1} \leq 1$ , reducing to  $W^2(\Lambda_{L|1}) = 1$  at  $\epsilon_{L|1}$ , where  $\Lambda_{L|1}^{-1} = \sigma$  reduces to a deterministic decoding correction. Figure 8 (left panel) summarizes this discussion. Generically, a large  $\epsilon_{L|1}$  corresponds to a non-deterministic decoding error, and the QP norm will generally be large in this regime, see Figure 8 (right panel) for an example based on the single-qubit depolarizing channel.

## 9. Mid-shot rejection

Mid-shot (MS) rejection corresponds to the simple termination of shots once the first rejected syndrome is measured, without waiting for the shot to end. Assuming the shot time is monotonically increasing in the circuit depth, this simple modification reduces the average time per shot, and therefore improves the QPU time overhead relative to (post-shot) rejection, though the shot overhead is unchanged. Thus, even though rejection always increases the shot overhead within SALEM (Eq. (29)), MS rejection within SALEM can sometimes reduce the QPU time.

For a quantitative analysis, we assume that the shot time is given by  $t_s = t_g t$ , where  $t_g$  is the time per logical layer, and  $t$  is the number of logical layers performed before the shot is rejected. Each logical layer contains  $w$  logical gates (the 'circuit width'), and the circuit volume

is given by  $V = wD$ , where  $D$  is the circuit depth (number of layers). Denoting the acceptance probability for each logical gate by  $p_{acc}$ , the average time per shot (in units of  $t_g$ ) with MS rejection is

$$\mathbb{E}[t] = Dp_{acc}^{wD} + (1 - p_{acc}^w) \sum_{t=1}^D tp_{acc}^{w(t-1)} = \frac{1 - p_{acc}^{wD}}{1 - p_{acc}^w}, \quad (40)$$

where  $D$  is the circuit depth.

The expected QPU time for an  $N$ -shot experiment is  $T_{MS} = N\mathbb{E}[t]$ , which should be compared with the total time  $T = ND$  without MS rejection. We therefore replace the shot overhead  $\Gamma_{rej} = \mathbb{P}_{acc}^{-1} = p_{acc}^{-wD}$  for rejection, with the QPU time overhead

$$\Gamma_{MS\ rej} = \mathbb{P}_{acc}^{-1} \mathbb{E}[t]/D = \frac{1 - p_{acc}^{wD}}{Dp_{acc}^{wD}(1 - p_{acc}^w)} \quad (41)$$

for MS rejection. To quantify this in terms of blowup rates, we compute

$$\begin{aligned} \lambda_{MS\ rej} &= \frac{1}{V\epsilon_L p_{rej|L}} \log \Gamma_{MS\ rej} \quad (42) \\ &= \frac{1}{V\epsilon_L p_{rej|L}} \log \left( \frac{1 - p_{acc}^{wD}}{Dp_{acc}^{wD}(1 - p_{acc}^w)} \right) \\ &= \frac{1}{vp_{rej|L}^w} \log \left( \frac{\epsilon_{L|rej}}{p_{rej|L}^w} \left( e^{\frac{p_{rej|L}^w v}{\epsilon_{L|rej}}} - 1 \right) \right) + O(\epsilon_L), \end{aligned}$$

where, in the last line, we set  $D = v/w\epsilon_L$  and  $p_{rej} = 1 - p_{acc} = p_{1|L}\epsilon_L/\epsilon_{L|1}$ , before expanding in  $\epsilon_L$ . Note that  $v = V\epsilon_L$  can be thought of as a total logical infidelity, or as a normalized volume, and must be  $O(1)$  for LEM to produce high accuracy estimators in reasonable time.

Comparing  $\lambda_{MS\ rej}$  to  $\lambda_{Rej} = 1/\epsilon_{L|1}$ , we define the ratio

$$r = \lambda_{MS\ rej}/\lambda_{Rej} = u^{-1} \log [u^{-1} (e^u - 1)] + O(\epsilon_L), \quad (43)$$

which, at leading order in  $\epsilon_L$ , is a function of a single parameter  $u = vp_{rej|L}/\epsilon_{L|rej}$ . Since useful partitions of syndromes satisfy  $\epsilon_{L|rej} \sim p_{rej|L}$  (see Fig. 3), one can think of  $u$  as a proxy for  $v$ :  $u \sim v$ . The function in Eq. (43) monotonically increases from 1/2 to 1, as  $u$  goes from 0 to  $\infty$ , see Fig. 9. Thus, MS rejection can reduce the blowup rate due to rejection by a factor of up to 2, depending on the value of  $u$ .

One may be concerned that the leading order ratio  $r(u)$  in Eq. (43) is independent of the aspect ratio of the circuit,  $w/D$ , though it's clear that MS rejection cannot give an advantage over post-shot rejection if the aspect ratio is too large (for  $D = 1$ ,  $\Gamma_{MS\ rej} = \Gamma_{rej}$ ). Nevertheless, Fig. 9 shows that the leading order expression accurately captures the behavior of  $r$  in the practically relevant regime of (i) circuits with aspect ratios as large as  $\sim 10^3$  (most quantum algorithms have aspect ratios  $\ll 1$ ), and (ii) circuits with volume  $v \sim 1 - 10$ , where the QPU time overhead for LEM is on one hand a limiting factor (and therefore important to reduce), but on the other hand feasible.

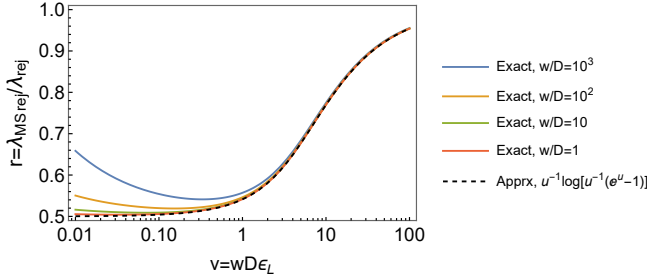


FIG. 9. Ratio of the blow-up rates  $\lambda_{MS\ rej}$  and  $\lambda_{rej}$  for mid-shot rejection and (post-shot) rejection, as a function of the total infidelity  $v = V\epsilon_L$ , based on Eq. (42)-(43). We set  $\epsilon_L = 10^{-6}$ ,  $f_{rej|L} = \epsilon_{L|rej} = 1/2$ , though the qualitative behavior is unchanged as long as  $\epsilon_L \ll 1$  and  $f_{rej|L} \sim \epsilon_{L|rej}$ . The different colors indicate different aspect ratios  $w/D$  (width/depth), while the black dashed line indicates a one-parameter, aspect-ratio-independent, approximation. Mid-shot rejection reduces the blowup rate due to rejection by a significant factor  $\approx 0.5 - 0.8$  for challenging but feasible  $v \sim 1 - 10$ , even for very wide and shallow circuits. Moreover, the approximate expression is highly accurate in this practically relevant regime.

## 10. Numerical simulations

### a. Steane code

We use Steane's code, a  $[[7, 1, 3]]$  CSS code, to fully simulate the methods discussed above for the case of a single logical qubit memory.

For syndrome extraction, we employ the 1-FT scheme of Ref. [65]. This scheme uses one ancilla qubit to measure the syndrome and an additional ancilla to flag hook errors. The measurement procedure is adaptive and consists of flagged and unflagged rounds. In the first round, syndromes are measured sequentially using flagged gadgets. If a flag or nontrivial syndrome is detected, the round is terminated and *all* syndromes are subsequently measured using unflagged gadgets. If no such event occurs, the second round is skipped. Recovery is performed using a lookup table (LUT) that applies minimal-weight decoding conditioned on which gadget triggered the flag.

Our circuit-level noise model consists of a two-qubit depolarizing channel applied after each CNOT with probability  $\epsilon_{ph}$ , an  $X$  error occurring with probability  $\epsilon_{ph}/2$  after each reset operation, and an identical error applied before measurements of the two ancilla qubits. We assume noiseless state preparation and encoding and noiseless final measurements of the data qubits.

This code permits a direct P2LC per syndrome thanks to the small number of stabilizer group cosets, namely  $2^{7+1} = 256$ , the total number of syndromes (only 448), and the relatively small depth and width of the syndrome-extraction gadgets. These features enable us to use brute-force enumeration of all fault paths with weight  $\leq 2$ , that is, we consider all faults paths with one

input error together with a single internal fault, or no input error and two internal faults. Using this enumeration we compute the joint distribution  $\mathbb{P}(s, \sigma_{out} | \sigma_{in})$ , where  $\sigma_{in}$  and  $\sigma_{out}$  are coset representatives of the input and output Pauli operators, and  $s$  is the measured syndrome. This joint distribution fully characterizes the faulty EC cycle and, in particular, allows us to compute the logical channels described in Appendix 1.

In the memory case we have  $G_j = \mathcal{E}$  for all  $j$ , where  $\mathcal{E}$  denotes the faulty EC cycle, and  $g_j = I$ , for  $1 \leq j \leq V$ . Since we consider long sequences, we neglect the special first ( $j = 1$ ) and last ( $j = V$ ) cycles and approximate  $\tilde{\Lambda}_L^{(j)} \approx \tilde{\Lambda}_L$  for  $1 < j < V$ .

Following the P2LC procedure in Appendix 1, we compute

$$\tilde{\Lambda}_{out}^{\text{prev}} |c\rangle\langle c| := \mathcal{E} |c\rangle\langle c|, \quad (44)$$

that is,

$$\tilde{\Lambda}_{out}^{\text{prev}} = \tilde{\Lambda}_{out}^{(j-1)} = \sum_{\sigma_{out}} \left( \sum_s \mathbb{P}(s, \sigma_{out} | I_{in}) \right) \sigma_{out}, \quad (45)$$

from which we extract  $\tilde{\Lambda}_c^{\text{prev}} = \tilde{\Lambda}_c^{(j-1)}$ , the correctable component of  $\tilde{\Lambda}_{out}^{\text{prev}}$ .

Using Eq. (4) we obtain

$$\tilde{\Lambda}_{out}|c\rangle\langle c| := \tilde{\Lambda}_{out}^{(j)}|c\rangle\langle c| = \mathcal{E} \tilde{\Lambda}_c^{\text{prev}}|c\rangle\langle c|, \quad (46)$$

and from Eq. (5) we get

$$\tilde{\Lambda}_L|c\rangle\langle c| := \tilde{\Lambda}_L^{(j)}|c\rangle\langle c| = \mathcal{E}_0 \tilde{\Lambda}_{out}|c\rangle\langle c|, \quad (47)$$

where  $\mathcal{E}_0$  is the noiseless version of  $\mathcal{E}$ . The channel  $\tilde{\Lambda}_L$ , whose error probability we denote by  $\epsilon_L$ , is the one mitigated in the ExtLEM procedure.

For binary CG-SALEM with rejection, we proceed as follows. We first partition the syndromes into accepted and rejected subsets,  $S_0$  and  $S_1$ , respectively. To perform this partitioning, we use the previously defined  $\tilde{\Lambda}_{out}$ , but conditioned on the measured syndrome  $s$ . If we write  $\tilde{\Lambda}_c^{\text{prev}} = \sum_{\sigma} p_{\sigma}^{(c)} \sigma$ , then

$$\tilde{\Lambda}_{out|s} := \frac{\sum_{\sigma, \sigma'} \mathbb{P}(s, \sigma | \sigma') p_{\sigma'}^{(c)} \sigma}{\sum_{\alpha, \alpha'} \mathbb{P}(s, \alpha | \alpha') p_{\alpha'}^{(c)}}. \quad (48)$$

From this, we obtain the logical channel conditioned on  $s$  via  $\Lambda_{L|s}|c\rangle\langle c| := \mathcal{E}_0 \tilde{\Lambda}_{out|s}|c\rangle\langle c|$ , yielding a logical error rate  $\epsilon_{L|s}$ , which we use for syndrome partitioning. Given a logical error threshold  $\tau$ , we define

$$S_1 = \{ s : \epsilon_{L|s} > \tau \}.$$

To compute the logical channel  $\tilde{\Lambda}_L^{\{S_0, S_1\}}$ , we modify Eqs. (44), (46) and (47) to account for the fact that all cycles must have syndromes in  $S_0$ , and in particular cycles  $j-1, j$  and  $j+1$ . Accordingly, we condition on  $S_0$  in

$\mathcal{E}$  (cycle  $j-1$  is accepted), in  $\mathcal{E} \tilde{\Lambda}_c^{\text{prev}}$  (cycle  $j$  is accepted) and in  $\mathcal{E}_0 \tilde{\Lambda}_{out}$  (cycle  $j+1$  is accepted).

Fig. 10(a) compares the decay of  $\langle Z_L \rangle$  predicted by the characterization procedure described above with simulation results. The figure highlights the importance of accounting for both the past—namely, input errors—and the future—specifically, the fact that the subsequent cycle yields a syndrome belonging to a given subset. Neglecting either effect leads to significant under- or overestimation of the error probabilities in the characterized logical channels.

Fig. 10(b) shows the blowup rates of binary CG-SALEM with rejection as a function of the partition threshold  $\tau$ . The measured optimal blowup rate for  $(\text{Inv}_0, \text{Reg}_1)$  is 2.4, and is reduced to 1.86 for  $(\text{Inv}_0, \text{MS\_Reg}_1)$ . We observe good agreement between the measured rates and the rates predicted from our P2LC data. The predicted optimal value is 2.46 and is consistent with the predicted optimal value obtained for FG-SALEM with LUT decoder as depicted on the left in Fig. 11. Here we get a range of blowup rates corresponding to the unknown logical errors for the missing probability in the fault-path enumeration. The small variation of about 0.03 indicates that the effect of the missing fault-paths is negligible.

Fig. 12 shows results analogous to Fig. 2(a) but with a full stabilizer simulation of the error-corrected circuit (using `Stim`). The ‘SALEM’ curve corresponds to binary CG-SALEM with syndrome partition threshold of  $\tau = 0.2$  as found from the simulation in Fig. 10(b). The estimated values are consistent with ideal value of 1 and exhibit a significantly lower error relatively to ExtLEM.

### b. Surface codes

To study the interplay of SALEM with decoding, as well as its scaling to larger-distance codes, we consider logical memory circuits for the family of distance- $d$  (rotated) surface codes, for which several decoders are publicly available. Specifically, we use the fault-tolerant memory circuits implemented in `Stim` [79], with  $d$  rounds of syndrome measurement, together with the compatible minimum-weight perfect matching (MWPM) decoder provided by `PyMatching` [64], and the circuit-level tensor-network (TN) decoder constructed in Ref. [69].

We consider circuit-level noise models throughout, where each physical single-qubit (two-qubit) gate is followed by a single-qubit (two-qubit) depolarizing channel, and each physical  $Z$ -basis reset (measurement) operation is followed (preceded) by a bit-flip channel, where all channels have the same physical error rate  $\epsilon$ .

In contrast to our detailed simulations of the Steane code presented in Appendix 10a, the surface-code circuits considered here involve two simplifying assumptions: (i) Only flips of a single logical operator ( $Z_L$ ) are measured, reducing the logical error channel to a logical bit-flip channel, and (ii) a final ideal round of syn-

drome measurement is performed, the outcomes of which are fed to the decoder. This latter assumption removes correctable errors that would otherwise serve as input errors to subsequent rounds of EC. These simplifying assumptions do not allow for a simulations of deep memory circuits with repeated error correction, but they suffice for estimating the shot overheads in various versions of SALEM, as well as the overhead and bias in EC and EC+PS.

As discussed in Sec. IV, the syndrome-conditioned logical characterization needed for FG-SALEM is a hard computational problem. For the distance-3 surface code, we perform a brute-force syndrome-conditioned logical characterization, by enumerating all weight  $\leq 3$  combinations of independent physical errors (or faults). This allows for an accurate approximation of ML decoding, and of the blowup rate for FG-SALEM, see Fig. 13. Brute force enumeration quickly becomes intractable as the code distance grows, and we were not able to perform it to a high-enough accuracy for  $d > 3$ .

As discussed in Sec. V, for binary CG-SALEM the syndrome-conditioned characterization splits into two tractable computations problems - classification, and subset-conditioned characterization. We perform classification using two soft-output decoders, based on the MWPM and TN decoders. A simplified physical-to-logical characterization (P2LC) of the subset-conditioned channels  $\Lambda_{L|0}$  and  $\Lambda_{L|1}$  (and the subset probabilities  $\mathbb{P}(S_0), \mathbb{P}(S_1)$ ) is then performed by sampling and simulating fault-paths (using `Stim`), decoding with MWPM, and collecting a joint distribution over subsets and logical errors.

For the MWPM decoder, we follow Ref. [58, 67, 68] to obtain a weight gap  $\Delta w_s = |w_{0,s} - w_{1,s}|$ , where  $w_{0,s}$  ( $w_{1,s}$ ) is the minimal weight of a fault-path in the ‘no logical error’ (‘logical error’) sector, given the syndrome  $s$ . These minimal weights are obtained by adding the measured value  $l = 0, 1$  of the logical operator as an additional bit in the syndrome,  $s' = s \cup \{l\}$ , and forcing  $l$  to either 0 or 1. The logical recovery operation is given by  $R_s = Z_L^{l_s}$ , where  $l_s = \text{argmin}_l(w_l)$ , while the gap  $\Delta w_s$  indicates the confidence of the decoder in this recovery, with a larger gap indicating higher confidence. We perform partition based on the condition

$$e^{-\Delta w_s} > \tau_{MWPM}, \quad (49)$$

which defines the ‘bad’ set of syndromes  $S_1$ . The quantity  $e^{-\Delta w_s}$  takes values in  $[0, 1]$ , and can be understood as the ratio of probabilities between the most probable fault-path (identified by MWPM) given the syndrome, and the most probable fault-path given the syndrome in the opposite logical sector.

The soft-output of the TN decoder directly corresponds to an estimate of  $\epsilon_{L|s}$ . In Ref. [69], a ‘difference TN’  $Z_-$ , which estimates  $\mathbb{P}(l = 1 \& s) - \mathbb{P}(l = 0 \& s)$ , is used for decoding, such that  $l_s^{TN} = \text{Heaviside}(Z_-)$  defines the logical recovery operation. We use the TN decoder as a classifier, assuming decoding is performed with

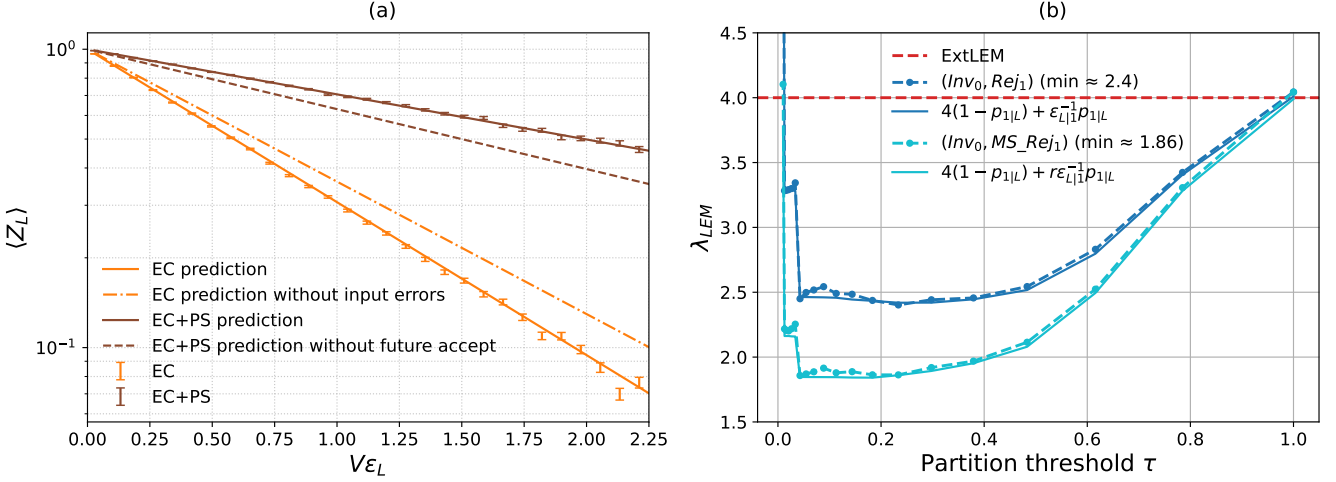


FIG. 10. Results for 1 logical qubit memory for Steane’s code. We consider a an initial logical state  $|0_L\rangle$  obtained by a noiseless encoder. In both plots we used  $\epsilon_{ph} = 4 \cdot 10^{-4}$  which gives  $\epsilon_L = 1.12 \cdot 10^{-4}$ . (a) Here we demonstrate the precision of the time-local characterization by comparing simulation results with our characterization predictions. The expectation value  $\langle Z \rangle$  decays as  $[1 - 2(p_x + p_y)]^V$ , where  $p_x$  and  $p_y$  are the probabilities of logical  $X_L$  and  $Y_L$  errors in  $\tilde{\Lambda}_L$  for EC, and in  $\tilde{\Lambda}_L^{\{S_0, S_1\}}$  for EC+PS. Error bars indicate the simulated values, while the solid curves show the predictions from our characterization. For EC, the dash-dot curve illustrates how neglecting input errors leads to a substantial *underestimation* of the logical error probabilities. For EC+PS, the dashed curve shows that failing to condition on acceptance in the subsequent cycle leads to a significant *overestimation* of the logical error probabilities. (b) Blowup rates for binary CG-SALEM with rejection and with mid-shot rejection. We find a good agreement between the dashed lines, correspond to the measured values, and the analytical solid curve. Here  $r$  is the factor defined in Eq. (43). We find optimal blowup rates at  $\tau \approx 0.2$ , with a significant improvement from mid-shot rejection, further reducing the optimal blowup rate from 2.4 to 1.86.

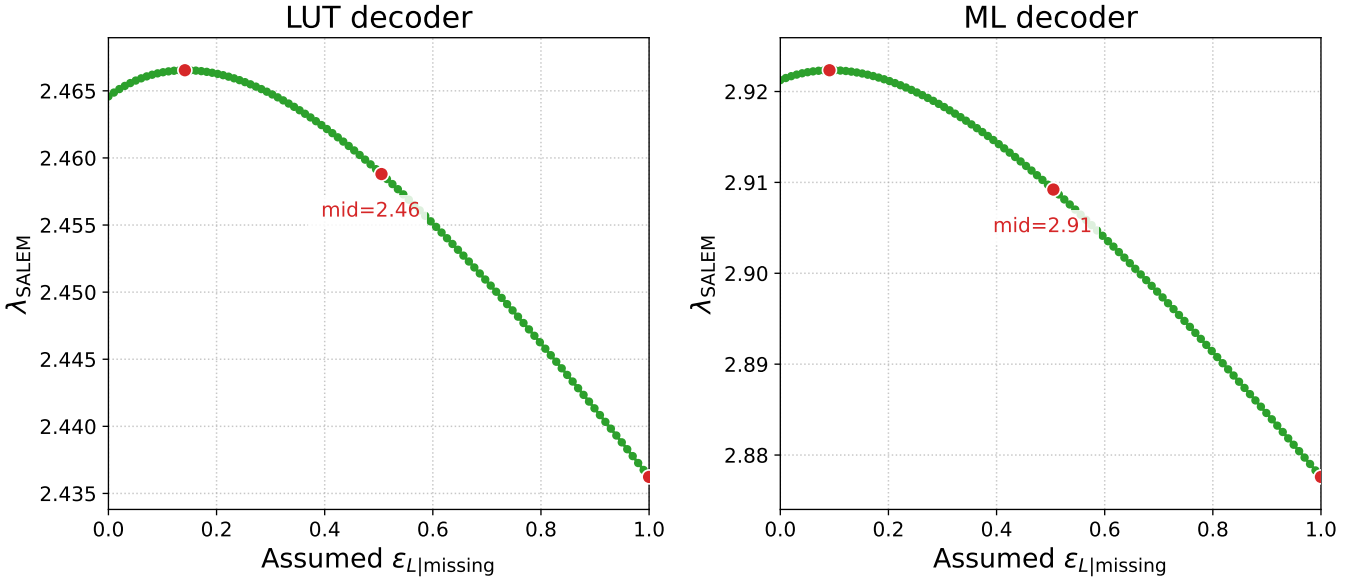


FIG. 11. Estimation of  $\lambda_{SALEM}^{FG}$  for Steane’s code. We use a brute-force enumeration of weight  $\leq 2$  fault-paths, and treat the missing probability, due to higher-weight faults-paths, as corresponding to a single additional syndrome, with unknown conditioned logical error  $\epsilon_{L|missing} \in [0, 1]$ . Red dots mark the minimal and maximal values obtained for  $\lambda_{SALEM}^{FG}$ , as well as the values obtained for  $\epsilon_{L|missing} = 1/2$ , assuming either the LUT decoder, or the ML decoder obtained by taking the logical error channel obtained for the LUT decoder, and applying the most probable logical error. The small changes in  $\lambda_{SALEM}^{FG}$  as a function of  $\epsilon_{L|missing}$  (note the scales of y-axes) indicate that higher-weight fault-paths have a negligible effect.

the weaker but faster MWPM. This is done by addition-

ally computing a TN  $Z_+$  which estimates  $\mathbb{P}(s) = \mathbb{P}(l =$

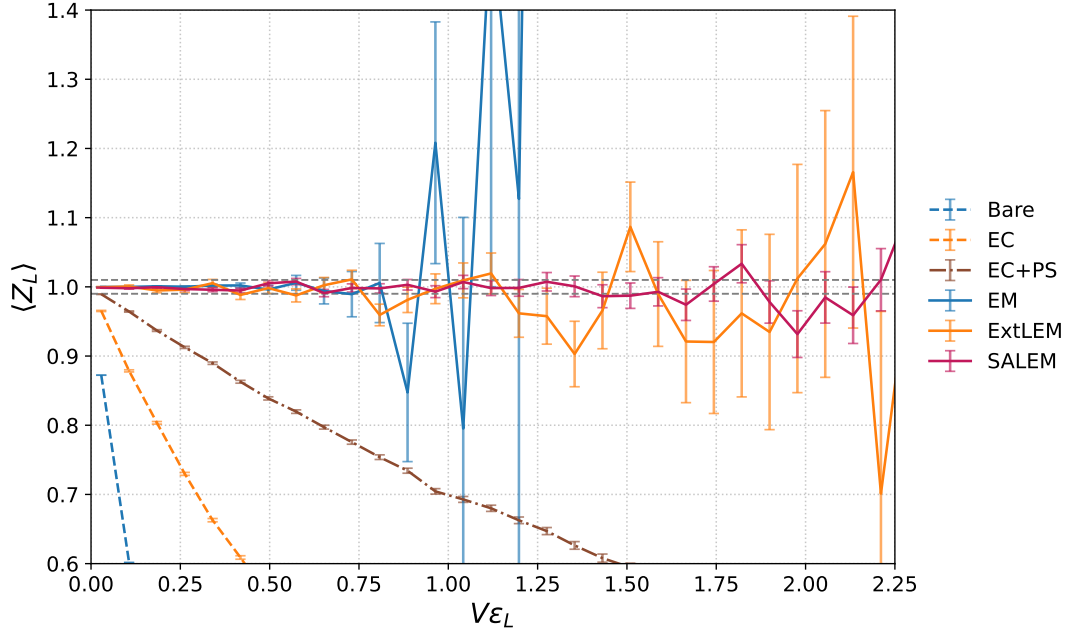


FIG. 12. Analog of Fig. 2(a) for Steane’s code. Here  $\epsilon_{ph} = 4 \cdot 10^{-4}$  which gives  $\epsilon_L = 1.12 \cdot 10^{-4}$ , and we consider memory circuits with lengths  $V$  between 256 and 20090. We simulate  $10^5$  shots for each value of  $V$ . The binary CG-SALEM with rejection is given by the “SALEM” curve and exhibits a significantly lower error relatively to ExtLEM and is unbiased. The rest of the curves are computed in the same way as in Fig. 2(a).

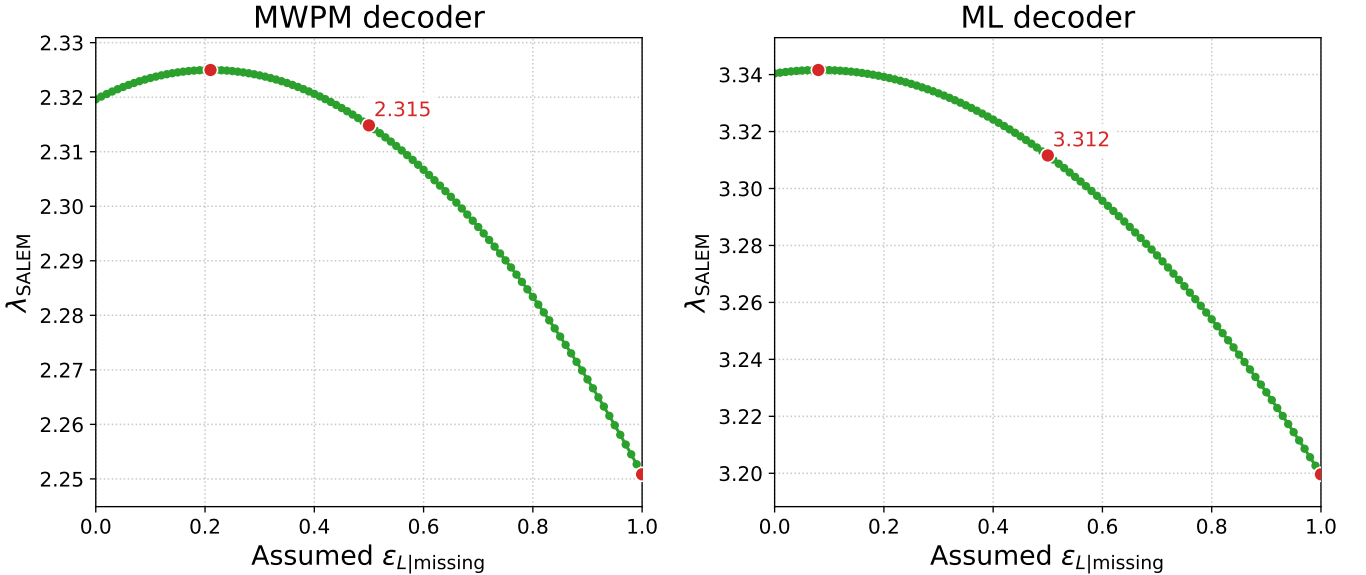


FIG. 13. Estimating  $\lambda_{SALEM}^{FG}$  for the  $d = 3$  surface code. We use a brute-force enumeration of weight  $\leq 3$  fault-paths, and treat the missing probability, due to higher-weight faults-paths, as corresponding to a single additional syndrome, with unknown conditioned logical error  $\epsilon_{L|missing} \in [0, 1]$ . Red dots mark the minimal and maximal values obtained for  $\lambda_{SALEM}^{FG}$ , as well as the values obtained for  $\epsilon_{L|missing} = 1/2$ , assuming either the MWPM decoder (left), or an approximation of the optimal ML decoder based on the same brute-force enumeration (right). The small changes in  $\lambda_{SALEM}^{FG}$  as a function of  $\epsilon_{L|missing}$  (note the scales of y-axes) indicate that higher-weight fault-paths have a negligible effect, and we use the values of  $\lambda_{SALEM}^{FG}$  obtained for  $\epsilon_{L|missing} = 1/2$  for Tab. I in the main text.

$1 \& s) + \mathbb{P}(l = 0 \& s)$ . We then obtain an estimate  $\tilde{\epsilon}_{L|s} = (1 + (-1)^{l_s} Z_- / Z_+)/2$  of  $\epsilon_{L|s}$ . Note that  $l_s$  cor-

responds to the recovery operation of MWPM, and not of the TN decoder. Binary partition is then performed

TABLE II. Simulation parameters used to generate Fig. 3, 14 and 15. The second group of parameters is relevant for TN classification, see Ref. [69] for details.

Parameter	$d = 3$	$d = 4$	$d = 5$
Physical error	0.001	0.002	0.007
Sampled fault-paths	$10^6$	$10^5$	$10^4$
Distinct syndromes	3,769	14,081	9,861
Truncation dimension	8	8	8
Bond dimension	20	12	12
MPS bond dimension	128	64	64
Split dimension	20	12	12
SVD cutoff	$10^{-12}$	$10^{-12}$	$10^{-12}$

based on the criterion

$$\tilde{\epsilon}_{L|s} > \tau_{TN}, \quad (50)$$

defining the ‘bad’ set  $S_1$ .

Note that we needed two TNs to perform classification, as opposed to just one needed for decoding. However, in the realistic case with  $4^k$  logical Paulis  $\sigma$  for  $k$  logical qubits, classification is easier than decoding. The latter requires  $4^k - 1$  TNs, corresponding to all non-zero Fourier components (with respect to  $\sigma$ ) of  $\mathbb{P}(\sigma \& s)$ , while the latter requires only two TNs (independent of  $k$ ), corresponding to  $\mathbb{P}(s)$  and  $\epsilon_{L\&s} = \mathbb{P}(\sigma \neq I \& s)$ .

The parameters we use to construct and contract TNs for  $d = 3, 4, 5$  are shown in Fig. II, along with the physical error rates, numbers of sampled fault-paths, and the number of distinct observed syndromes, which are decoded once to reduce runtime. As noted in Ref. [69], the authors did not focus on optimizing TN decoding runtime, which is excessive, with  $\sim 15$  hours of parallelized computation on a machine with 90 CPUs needed for  $d = 5$ . Results for  $d = 4$  are shown in Fig. 3, while results for  $d = 3, 5$  are shown in Fig. 14-15. We observe an even-odd effect with respect to code distance, where binary CG-SALEM blowup rates are smaller for even  $d$  than for odd  $d$ . This is rooted in the well-known ability of distance  $d = 2t + 2$  codes to correct  $t$  errors and additionally detect  $t + 1$  errors (implying a better performance of EC+PS), which suggests the existence of partitions with simultaneously larger  $\epsilon_{L|1}$  and  $p_{1|L}$  (see bottom panels in Fig. 3, 14,15).

To produce Fig. 2 in the main text, we use a particular binary CG-SALEM method for  $d = 4$ , defined by the optimal partition for  $(\text{Inv}_0, \text{MS\_Rej}_1)$  with the MWPM classifier (minimal point on the cyan line in Fig. 3, Top Left). We then perform three types of parameter scans, generating an estimate for the bias and standard deviation of Bare, EM, EC, ExtLEM, EC+PS and SALEM, for each parameter value. We refer to the sum of the bias and statistical error as a ‘total estimation error’. For Fig. 2(a), we scan over circuit volume  $V$ , and plot the estimated bias and standard deviation for each method as a function of  $V$  (data points and error bars are simply

obtained by sampling from corresponding normal distributions). For Fig. 2(b), we scan over the required accuracy  $1 - \delta$ , and identify the maximal volume for each method such that the total estimation error is  $\leq \delta$ . For Fig. 2(c), we scan over physical error rates  $\epsilon$  around the FT (pseudo) threshold, and plot the total estimation error as a function of  $\epsilon$ . For Fig. 2(a)-(b), we allocate a space-time volume corresponding to a total of  $10^4$  error-corrected shots, for all error reduction methods. For Fig. 2(c) we allocate a total of  $10^8$  error-corrected shots.

We set the bias to 0 for EM, ExtLEM and SALEM. The bias for Bare is  $1 - (1 - 4\epsilon/3)^V$ , corresponding to a physical depolarizing channel with parameter  $\epsilon$ . The shot overhead for EM is  $\Gamma = (1 - 4\epsilon/3)^{-2V}/V_{EC}$ , corresponding to mitigating only the  $X$  and  $Y$  errors which affect the measured  $Z$ , and we divide by the space-time overhead of error-correction  $V_{EC}$ , to account for the reduced time of physical shots compared to error-corrected shots, as well as EM’s ability to parallelize shots using multiple qubit patches, corresponding to the (net) rate of the code used. For the surface code, the net rate is  $1/(2d^2 - 1)$ , and each round of stabilizer measurements involves four layers of physical two-qubit gates and one layer of measurement and reset operations. We therefore take the space-time overhead per round to be  $V_{EC} = 5(2d^2 - 1) = 75$  for  $d = 4$ . All other biases and standard deviations are estimated using the simplified P2LC described above, where all quantities are computed per-round. In particular, the bias for EC is  $1 - (1 - 2\epsilon_L/d)^V$ , and the bias for EC+PS is  $1 - (1 - 2\epsilon_{L|0}/d)^V$ , both corresponding to logical bit-flip channels.

## 11. FT pseudo thresholds for ExtLEM and SALEM

We explain here the behavior of the FT (pseudo) thresholds for ExtLEM and SALEM described in the main text (Fig. 2(c)). The standard FT (pseudo) threshold is defined as the solution to  $\epsilon_L(\epsilon) = \epsilon$ . In contrast, the ExtLEM threshold is defined by equating the QPU time overheads of (physical) EM and ExtLEM:

$$V_{EC}e^{\lambda\epsilon_L(\epsilon)V} = \Gamma_{ExtLEM} = \Gamma_{EM} = e^{\lambda\epsilon V}, \quad (51)$$

where  $V_{EC}$  is the space-time overhead for EC, discussed in Appendix 10b, and we adopt an exponential form for the shot overhead, for simplicity. This can be written as

$$\frac{\log V_{EC}}{\lambda V} + \epsilon_L(\epsilon) = \epsilon, \quad (52)$$

which is identical to the defining equation of the FT threshold, but with a  $V$ -dependent addition to the logical error. It is therefore clear that the ExtLEM threshold is always lower than the FT threshold, and converges to it as  $V \rightarrow \infty$ . Similarly, the equation defining the SALEM threshold is

$$V_{EC}e^{\lambda_{SALEM}\epsilon_L(\epsilon)V} = \Gamma_{SALEM} = \Gamma_{EM} = e^{\lambda\epsilon V}, \quad (53)$$

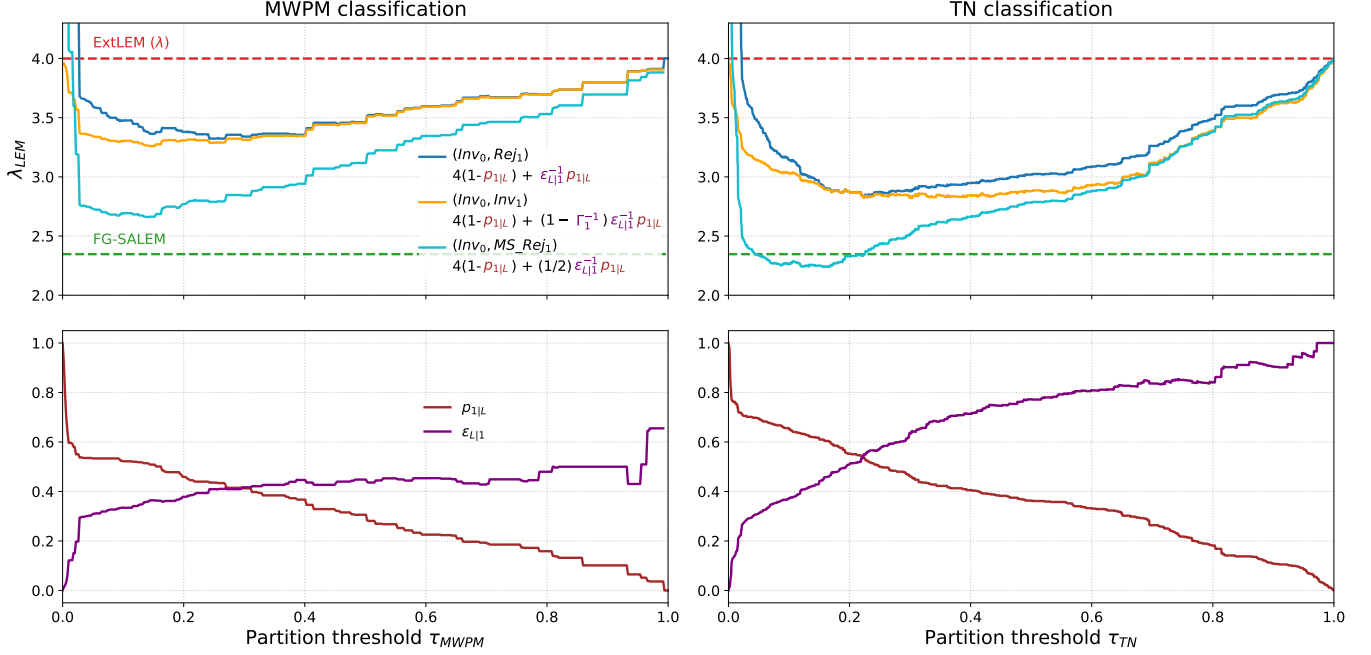


FIG. 14. Binary CG-SALEM for the  $d = 3$  surface code memory circuit. See Fig. 3 for details. Note that Mid-shot rejection can even improve the QPU time overhead (but not the shot overhead) over FG-SALEM.

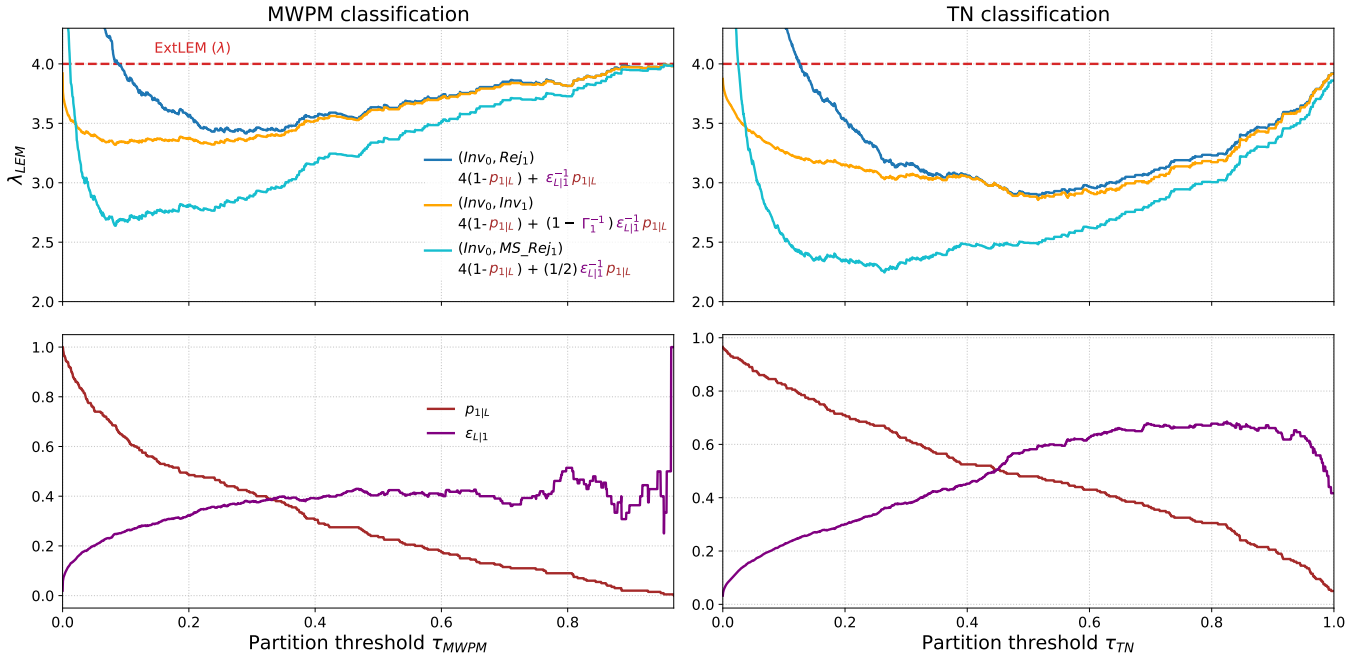


FIG. 15. Binary CG-SALEM for the  $d = 5$  surface code memory circuit. See Fig. 3 for details. The drop in  $\epsilon_{L|1}$  for  $\tau_{TN} > 0.8$  shows that the TN classifier we use struggles to approximate  $\epsilon_{L|s}$  for the ‘worst’ syndromes  $s$  where this quantity is close to 1. Nevertheless, the TN classifier approximates  $\epsilon_{L|s}$  well enough to produce strong partitions, which significantly improve the blowup rate for binary CG-SALEM relative to the MWPM classifier. Optimal blowup rates with both classifiers and all three variants of binary CG-SALEM are close to those observed for  $d = 3$ .

such that

$$\frac{\log V_{EC}}{\lambda V} + \frac{\lambda_{SALEM}}{\lambda} \epsilon_L(\epsilon) = \epsilon. \quad (54)$$

Since  $\lambda_{SALEM} < \lambda$ , it’s clear that the SALEM threshold is always higher than the ExtLEM threshold and that, as  $V \rightarrow \infty$ , we obtain a SALEM threshold which

is higher than the FT threshold. On the other hand, at small volume, the first term dominates. To identify the transition, parametrize  $V = v/\epsilon_L(\epsilon)$ . The SALEM threshold is higher than the FT threshold if  $v > v_0 = \log V_{EC}/(\lambda - \lambda_{SALEM})$ . As discussed above, for surface codes of distance  $d$  we have  $V_{EC} = 5(2d^2 - 1)$ . Thus,  $\log(V_{EC})$  is, say,  $< 10$  up to very high code distances

$\approx 60$ , and considering values of  $\lambda - \lambda_{SALEM}$  presented here, it is expected that volumes that reach this regime above the FT threshold but below the SALEM threshold, namely  $V > v_0/\epsilon_L$  are feasible for SALEM with reasonable QPU time overhead. Note that in Fig. 2(c) we used the convention  $V = v/\epsilon$  as opposed to  $V = v/\epsilon_L(\epsilon)$ .

---

[1] D. W. Berry, R. S. T. Oliver, L. M. D. Ashley, and D. M. W. P. Brown, Quantum algorithm zoo, <https://quantumalgorithmzoo.org/> (2020), accessed: 2025-02-16.

[2] D. Aharonov and M. Ben-Or, Fault-tolerant quantum computation with constant error rate, in *Proceedings of the 29th Annual ACM Symposium on Theory of Computing* (ACM, 1997) pp. 176–188.

[3] E. Knill, R. Laflamme, and W. H. Zurek, Resilient quantum computation: error models and thresholds, *Proceedings of the Royal Society of London. Series A: Mathematical, Physical and Engineering Sciences* **454**, 365–384 (1998).

[4] A. Kitaev, Quantum computations: algorithms and error correction, *Russian Mathematical Surveys* **52**, 1191 (1997).

[5] P. Aliferis, D. Gottesman, and J. Preskill, Accuracy threshold for postselected quantum computation (2007), arXiv:quant-ph/0703264 [quant-ph].

[6] A. Peres, Reversible logic and quantum computers, *Phys. Rev. A* **32**, 3266 (1985).

[7] P. W. Shor, Scheme for reducing decoherence in quantum computer memory, *Physical Review A* **52**, R2493 (1995).

[8] A. M. Steane, Error correcting codes in quantum theory, *Physical Review Letters* **77**, 793 (1996).

[9] Error Correction Zoo Contributors, The error correction zoo, <https://errorcorrectionzoo.org> (2020), online resource.

[10] D. Bluvstein, S. J. Evered, A. A. Geim, S. H. Li, H. Zhou, T. Manovitz, S. Ebadi, M. Cain, M. Kalinowski, D. Hangleiter, *et al.*, Logical quantum processor based on reconfigurable atom arrays, *Nature* **626**, 58 (2024).

[11] M. da Silva, C. Ryan-Anderson, J. Bello-Rivas, A. Chernoguzov, J. Dreiling, C. Foltz, F. Frachon, J. Gaebler, T. Gatterman, L. Grans-Samuelsson, *et al.*, Demonstration of logical qubits and repeated error correction with better-than-physical error rates (2024), arXiv preprint arXiv:2404.02280 .

[12] B. W. Reichardt, D. Aasen, R. Chao, A. Chernoguzov, W. van Dam, J. P. Gaebler, D. Gresh, D. Lucchetti, M. Mills, S. A. Moses, *et al.*, Demonstration of quantum computation and error correction with a tesseract code, arXiv preprint arXiv:2409.04628 (2024).

[13] R. Acharya, L. Aghababaie-Beni, I. Aleiner, T. I. Andersen, M. Ansmann, F. Arute, K. Arya, A. Asfaw, N. Astrakhantsev, J. Atalaya, *et al.*, Quantum error correction below the surface code threshold, arXiv preprint arXiv:2408.13687 (2024).

[14] H. Puterman, K. Noh, C. T. Hann, G. S. MacCabe, S. Aghaeimeibodi, R. N. Patel, M. Lee, W. M. Jones, H. Moradinejad, R. Rodriguez, *et al.*, Hardware-efficient quantum error correction using concatenated bosonic qubits, arXiv preprint arXiv:2409.13025 (2024).

[15] G. M. Sommers, M. Foss-Feig, D. Hayes, D. A. Huse, and M. J. Gullans, Observation of a fault tolerance threshold with concatenated codes, *Phys. Rev. Res.* **7**, 043271 (2025).

[16] A. Eickbusch, M. McEwen, A. Morvan, B. Ware, T. Weidel, T. White, K. Wong, B. W. K. Woo, M. Woodson, C. Xing, *et al.*, Demonstration of dynamic surface codes, *Nature Physics* **21**, 1994 (2025).

[17] P. S. Rodriguez, J. M. Robinson, P. N. Jepsen, Z. He, C. Duckering, C. Zhao, K.-H. Wu, J. Campo, K. Bagnall, M. Kwon, *et al.*, Experimental demonstration of logical magic state distillation, *Nature* **645**, 620 (2025).

[18] K. Yamamoto, Y. Kikuchi, D. Amaro, B. Criger, S. Dilkes, C. Ryan-Anderson, A. Tranter, J. M. Dreiling, D. Gresh, C. Foltz, *et al.*, Quantum error-corrected computation of molecular energies, arXiv preprint arXiv:2505.09133 10.48550/arXiv.2505.09133 (2025).

[19] D. Bluvstein, A. A. Geim, S. H. Li, S. J. Evered, J. P. Bonilla Ataides, G. Baranes, A. Gu, T. Manovitz, M. Xu, M. Kalinowski, and collaborators, A fault-tolerant neutral-atom architecture for universal quantum computation, *Nature* **10.1038/s41586-025-09848-5** (2025).

[20] Q. Xu, J. P. Bonilla Ataides, C. A. Pattison, N. Raveendran, D. Bluvstein, J. Wurtz, B. Vasić, M. D. Lukin, L. Jiang, and H. Zhou, Constant-overhead fault-tolerant quantum computation with reconfigurable atom arrays, *Nature Physics* **1** (2024).

[21] S. Bravyi, A. W. Cross, J. M. Gambetta, D. Maslov, P. Rall, and T. J. Yoder, High-threshold and low-overhead fault-tolerant quantum memory, *Nature* **627**, 78 (2024), accessed: 2024-10-21.

[22] T. R. Scruby, T. Hillmann, and J. Roffe, High-threshold, low-overhead and single-shot decodable fault-tolerant quantum memory, arXiv preprint arXiv:2406.14445 (2024).

[23] C. Gidney, N. Shutty, and C. Jones, Magic state cultivation: growing t states as cheap as cnot gates, arXiv preprint arXiv:2409.17595 (2024).

[24] Google Quantum AI, Google Quantum AI (2024), accessed: 2024-10-21.

[25] IBM Quantum, Ibm quantum technology (2024), accessed: 2024-10-21.

[26] QuEra Computing, Quera quantum error correction (qec) (2024), accessed: 2024-10-21.

[27] Quantinuum, Quantinuum Unveils Accelerated Roadmap to Achieve Universal Fault-Tolerant Quantum Computing by 2030 (2023), accessed: 2024-10-21.

[28] IonQ, Ionq unveils accelerated roadmap and new technical milestones to propel quantum computing (2024), accessed: 2024-10-21.

[29] IQM Quantum Computers, [Iqm quantum computers technology roadmap](#) (2024), accessed: 2024-10-21.

[30] D. Aharonov, O. Alberton, I. Arad, Y. Atia, E. Bairey, Z. Brakerski, I. Cohen, O. Golan, I. Gurwich, O. Kenneth, *et al.*, On the importance of error mitigation for quantum computation, [arXiv preprint arXiv:2503.17243](#) (2025).

[31] J. Preskill, Beyond nisq: The megaquop machine, *ACM Transactions on Quantum Computing* **10**.1145/3723153 (2025), just Accepted.

[32] K. Temme, S. Bravyi, and J. M. Gambetta, Error mitigation for short-depth quantum circuits, *Phys. Rev. Lett.* **119**, 180509 (2017).

[33] Y. Li and S. C. Benjamin, Efficient variational quantum simulator incorporating active error minimization, *Physical Review X* **7**, 021050 (2017).

[34] S. Endo, S. C. Benjamin, and Y. Li, Practical quantum error mitigation for near-future applications, *Phys. Rev. X* **8**, 031027 (2018).

[35] Z. Cai, R. Babbush, S. C. Benjamin, S. Endo, W. J. Huggins, Y. Li, J. R. McClean, and T. E. O'Brien, Quantum error mitigation, *Rev. Mod. Phys.* **95**, 045005 (2023).

[36] A. Mari, N. Shammah, and W. J. Zeng, Extending quantum probabilistic error cancellation by noise scaling, *Phys. Rev. A* **104**, 052607 (2021).

[37] Z. Cai, Multi-exponential error extrapolation and combining error mitigation techniques for nisq applications, *npj Quantum Information* **7**, 80 (2021).

[38] S. N. Filippov, S. Maniscalco, and G. García-Pérez, Scalability of quantum error mitigation techniques: from utility to advantage, [arXiv preprint arXiv:2403.13542](#) (2024).

[39] Z. Zimborás, B. Koczor, Z. Holmes, E.-M. Borrelli, A. Gilyén, H.-Y. Huang, Z. Cai, A. Acín, L. Aolita, L. Banchi, *et al.*, Myths around quantum computation before full fault tolerance: What no-go theorems rule out and what they don't, [arXiv preprint arXiv:2501.05694](#) (2025).

[40] O. Lanes, M. Beji, A. D. Corcoles, C. Dalyac, J. M. Gambetta, L. Henriet, A. Javadi-Abhari, A. Kandala, A. Mezzacapo, C. Porter, *et al.*, A framework for quantum advantage, [arXiv preprint arXiv:2506.20658](#) (2025).

[41] D. Aharonov, O. Alberton, I. Arad, Y. Atia, E. Bairey, M. B. Dov, A. Berkovitch, Z. Brakerski, I. Cohen, E. Fuchs, *et al.*, Reliable high-accuracy error mitigation for utility-scale quantum circuits, [arXiv preprint arXiv:2508.10997](#) (2025).

[42] J. Eisert and J. Preskill, Mind the gaps: The fraught road to quantum advantage, [arXiv preprint arXiv:2510.19928](#) [10.48550/arXiv.2510.19928](#) (2025), [arXiv:2510.19928](#) [quant-ph].

[43] Y. Kim, A. Eddins, S. Anand, K. X. Wei, E. Van Den Berg, S. Rosenblatt, H. Nayfeh, Y. Wu, M. Zaletel, K. Temme, *et al.*, Evidence for the utility of quantum computing before fault tolerance, *Nature* **618**, 500 (2023).

[44] R. Haghshenas, E. Chertkov, M. Mills, W. Kadow, S.-H. Lin, Y.-H. Chen, C. Cade, I. Niesen, T. Bećušić, M. S. Rudolph, *et al.*, Digital quantum magnetism at the frontier of classical simulations, [arXiv preprint arXiv:2503.20870](#) (2025).

[45] Google Quantum AI and Collaborators, Observation of constructive interference at the edge of quantum ergodicity, *Nature* **646**, 825 (2025).

[46] F. Alam, J. L. Bosse, I. Čepaitė, A. Chapman, L. Clinton, M. Crichigno, E. Crosson, T. Cubitt, C. Derby, O. Dowintor, *et al.*, Fermionic dynamics on a trapped-ion quantum computer beyond exact classical simulation, [arXiv preprint arXiv:2510.26300](#) (2025).

[47] R. Takagi, S. Endo, S. Minagawa, and M. Gu, Fundamental limits of quantum error mitigation, *npj Quantum Information* **8**, 114 (2022).

[48] R. Takagi, H. Tajima, and M. Gu, Universal sampling lower bounds for quantum error mitigation, *Phys. Rev. Lett.* **131**, 210602 (2023).

[49] K. Tsubouchi, T. Sagawa, and N. Yoshioka, Universal cost bound of quantum error mitigation based on quantum estimation theory, *Phys. Rev. Lett.* **131**, 210601 (2023).

[50] Y. Quek, D. Stilck França, S. Khatri, J. J. Meyer, and J. Eisert, Exponentially tighter bounds on limitations of quantum error mitigation, *Nature Physics* **20**, 1648 (2024).

[51] T. Schuster, C. Yin, X. Gao, and N. Y. Yao, A polynomial-time classical algorithm for noisy quantum circuits, [arXiv preprint arXiv:2407.12768](#) (2024).

[52] Y. Suzuki, S. Endo, K. Fujii, and Y. Tokunaga, Quantum error mitigation as a universal error reduction technique: Applications from the nisq to the fault-tolerant quantum computing eras, *PRX Quantum* **3**, 010345 (2022).

[53] C. Piveteau, D. Sutter, S. Bravyi, J. M. Gambetta, and K. Temme, Error mitigation for universal gates on encoded qubits, *Phys. Rev. Lett.* **127**, 200505 (2021).

[54] M. Lostaglio and A. Ciani, Error mitigation and quantum-assisted simulation in the error corrected regime, *Phys. Rev. Lett.* **127**, 200506 (2021).

[55] Y. Xiong, D. Chandra, S. X. Ng, and L. Hanzo, Sampling overhead analysis of quantum error mitigation: Uncoded vs. coded systems, *IEEE Access* **8**, 228967 (2020).

[56] K. Tsubouchi, Y. Mitsuhashi, K. Sharma, and N. Yoshioka, Symmetric clifford twirling for cost-optimal quantum error mitigation in early ftqc regime, [arXiv preprint arXiv:2405.07720](#) (2024).

[57] A. Zhang, H. Xie, Y. Gao, J.-N. Yang, Z. Bao, Z. Zhu, J. Chen, N. Wang, C. Zhang, J. Zhong, *et al.*, Demonstrating quantum error mitigation on logical qubits, [arXiv preprint arXiv:2501.09079](#) (2025).

[58] S. C. Smith, B. J. Brown, and S. D. Bartlett, Mitigating errors in logical qubits, *Communications Physics* **7**, 386 (2024).

[59] P. Prabhu and B. W. Reichardt, Distance-four quantum codes with combined postselection and error correction, *Phys. Rev. A* **110**, 012419 (2024).

[60] E. Van Den Berg, Z. K. Minev, A. Kandala, and K. Temme, Probabilistic error cancellation with sparse pauli-lindblad models on noisy quantum processors, *Nature physics* **19**, 1116 (2023).

[61] S. Filippov, M. Leahy, M. A. Rossi, and G. García-Pérez, Scalable tensor-network error mitigation for near-term quantum computing, [arXiv preprint arXiv:2307.11740](#) (2023).

[62] IBM Quantum, Propagated noise absorption, <https://qiskit.github.io/qiskit-addon-pna/> (2024), qiskit add-on for error mitigation using Pauli propagation.

[63] A. deMarti iOlius, P. Fuentes, R. Orús, P. M. Crespo, and J. Etxezarreta Martinez, Decoding algorithms for surface codes, *Quantum* **8**, 1498 (2024).

[64] O. Higgott, [Pymatching: A python package for decoding quantum codes with minimum-weight perfect matching](#) (2021), arXiv:2105.13082v2, [arXiv:2105.13082](#) [quant-ph].

[65] R. Chao and B. W. Reichardt, Quantum error correction with only two extra qubits, *Physical Review Letters* **121**, 10.1103/physrevlett.121.050502 (2018).

[66] P. Iyer and D. Poulin, Hardness of decoding quantum stabilizer codes, *IEEE Transactions on Information Theory* **61**, 5209 (2015).

[67] N. Meister, C. A. Patterson, and J. Preskill, Efficient soft-output decoders for the surface code, [arXiv preprint arXiv:2405.07433](#) (2024).

[68] C. Gidney, M. Newman, P. Brooks, and C. Jones, Yoked surface codes, *Nature Communications* **16**, 4498 (2025).

[69] C. Piveteau, C. T. Chubb, and J. M. Renes, Tensor network decoding beyond 2d, [arXiv preprint arXiv:2310.10722](#) (2023), last revised Oct 8 2024.

[70] R. Toshio, K. Kishi, J. Fujisaki, H. Oshima, S. Sato, and K. Fujii, Decoder switching: Breaking the speed-accuracy tradeoff in real-time quantum error correction, [arXiv preprint arXiv:2510.25222](#) (2025).

[71] Qedma Quantum Computing Ltd., Mitigation and characterization of logical errors in error corrected quantum processors (2024), also filed as US 19/343,333.

[72] K. Mayer, C. Ryan-Anderson, N. Brown, E. Durso-Sabina, C. H. Baldwin, D. Hayes, J. M. Dreiling, C. Foltz, J. P. Gaebler, T. M. Gatterman, *et al.*, Benchmarking logical three-qubit quantum fourier transform encoded in the steane code on a trapped-ion quantum computer, [arXiv preprint arXiv:2404.08616](#) (2024).

[73] A. Ransford, M. S. Allman, *et al.*, Helios: A 98-qubit trapped-ion quantum computer, [arXiv preprint arXiv:2511.05465](#) (2025).

[74] A. Kaufmann and I. Arad, A blockbp decoder for the surface code, [arXiv preprint arXiv:2402.04834](#) (2024).

[75] Z. Zhou, S. Pexton, A. Kubica, and Y. Ding, Error mitigation of fault-tolerant quantum circuits with soft information, [arXiv preprint arXiv:2512.09863](#) (2025).

[76] M. Dincă, T. Chan, and S. C. Benjamin, Error mitigation for logical circuits using decoder confidence (2025), [arXiv:2512.15689](#) [quant-ph].

[77] D. Gottesman, An introduction to quantum error correction and fault-tolerant quantum computation, [arXiv preprint arXiv:0904.2557](#) (2009).

[78] P.-J. H. S. Derkx, A. Townsend-Teague, A. G. Burchards, and J. Eisert, Designing fault-tolerant circuits using detector error models, [arXiv preprint arXiv:2407.13826](#) (2024).

[79] C. Gidney, Stim: a fast stabilizer circuit simulator, *Quantum* **5**, 497 (2021), [arXiv:2103.02202](#).